INVESTIGATION OF FLOW PATTERNS AND MEASUREMENT OF ACTUAL BUBBLE VELOCITY USING VOID FRACTION PROFILE IN A VERTICAL INDUSTRIAL SCALE TWO-PHASE FLOW CHANNEL

NUR ADANIA BINTI NOR AZMAN

FACULTY OF ENGINEERING
UNIVERSITY OF MALAYA
KUALA LUMPUR

2022

INVESTIGATION OF FLOW PATTERNS AND MEASUREMENT OF ACTUAL BUBBLE VELOCITY USING VOID FRACTION PROFILE IN A VERTICAL INDUSTRIAL SCALE TWO-PHASE FLOW CHANNEL

NUR ADANIA BINTI NOR AZMAN

THESIS SUBMITTED IN FULFILMENT OF THE REQUIREMENTS FOR THE DEGREE OF MASTER IN MECHANICAL ENGINEERING

DEPARTMENT OF MECHANICAL ENGINEERING
FACULTY OF ENGINEERING
UNIVERSITY OF MALAYA
KUALA LUMPUR

2022

UNIVERSITY OF MALAYA
ORIGINAL LITERARY WORK DECLARATION

Name of Candidate: Nur Adania Binti Nor Azman

Matric No: S2012241

Name of Degree: Masters in Mechanical Engineering

Title of Project Paper/Research Report/Dissertation/Thesis ("this Work"): Investigation Of Flow Patterns And Measurement Of Actual Bubble Velocity Using Void Fraction Profile In A Vertical Industrial Scale Two-Phase Flow Channel

Field of Study: Mechanical Engineering

I do solemnly and sincerely declare that:

(1) I am the sole author/writer of this Work;
(2) This Work is original;
(3) Any use of any work in which copyright exists was done by way of fair dealing and for permitted purposes and any excerpt or extract from, or reference to or reproduction of any copyright work has been disclosed expressly and sufficiently and the title of the Work and its authorship have been acknowledged in this Work;
(4) I do not have any actual knowledge nor do I ought reasonably to know that the making of this work constitutes an infringement of any copyright work;
(5) I hereby assign all and every rights in the copyright to this Work to the University of Malaya ("UM"), who henceforth shall be owner of the copyright in this Work and that any reproduction or use in any form or by any means whatsoever is prohibited without the written consent of UM having been first had and obtained;
(6) I am fully aware that if in the course of making this Work I have infringed any copyright whether intentionally or otherwise, I may be subject to legal action or any other action as may be determined by UM.

Candidate's Signature Date: 23/2/2022

Subscribed and solemnly declared before,

Witness's Signature Date: 23/2/2022

Name:

Designation:

ABSTRACT

Measurement of void fraction for two-phase flows involving gas and liquid in a vertical channel have been extensively researched to improve cooling system designs for energy-related industries and process refineries. Void fraction is the representation of gas and liquid ratio in a flow channel at certain working conditions. Using the Constant Electric Current Method (CECM), void fractions were obtained using sensor electrodes connected to data acquisition (DAQ) hardware which outputs the results to LabVIEW® software. Three sets of experiment were run at three fixed liquid superficial velocities, j_L, at 0.071-m/s, 0.227-m/s and 0.397-m/s with varying gas superficial velocities, j_G, ranging between 0-m/s to 0.3979-m/s. Utilizing the data captured, the objectives of this study were achieved by comparing the relationship of void fractions, flow patterns and actual bubble velocities in two-phase flows. At a constant liquid superficial velocity, the value of void fraction is found to increase with increasing gas superficial velocities which showed similar trend with other researchers' discoveries. In addition, maximum void fraction was obtained with the lowest liquid superficial velocity and highest gas superficial velocity. Conforming to the void fraction trend, flow patterns that were captured with a high-speed camera demonstrated that bubbly flow, slug flow and churn flow exist for these experiments. In addition, the actual bubble velocity calculated, yielded maximum value when liquid superficial velocity and gas superficial velocity is at the highest. In short, this project conforms to existing literature and could be developed further to determine dryout location in a vertical tube based on the actual bubble velocity.

ABSTRAK

Pecahan lompang untuk aliran dua fasa yang melibatkan gas dan cecair dalam saluran menegak telah dikaji secara meluas untuk menambah baik reka bentuk sistem penyejukan untuk industry tenaga dan kilang proses penapisan. Pecahan lompang ialah perwakilan nisbah gas dan cecair dalam saluran aliran pada ketetapan kerja tertentu. Menggunakan Kaedah Arus Elektrik Malar (CECM), pecahan lompang diperoleh menggunakan elektrod penderia yang disambungkan pada perkakasan pemerolehan data (DAQ) yang mempamerkan keputusan di LabVIEW®. Tiga set eksperimen dijalankan pada tiga halaju cecair dangkal tetap, j_L, pada 0.071-m/s, 0.227-m/s dan 0.397-m/s dengan halaju gas dangkal, j_G, yang berbeza-beza antara 0-m/s hingga 0.3979 -m/s. Dengan menggunakan data yang diperoleh, objektif-objektif kajian ini dicapai dengan membandingkan hubungan pecahan lompang, corak aliran dan halaju sebenar buih dalam aliran dua fasa. Pada halaju cecair dangkal yang berterusan, nilai pecahan lompang didapati meningkat dengan peningkatan halaju gas dangkal, menunjukkan trend yang sama dengan penemuan penyelidik lain. Selain itu, pecahan lompang maksimum diperoleh dengan halaju cecair dangkal terendah dan halaju gas dangkal tertinggi. Serupa dengan keputusan pecahan lompang, corak aliran yang direkod menggunakan kamera berkelajuan tinggi menunjukkan bahawa aliran berbuih, aliran slug dan aliran churn wujud untuk eksperimen ini. Di samping itu, halaju sebenar buih yang dikira, menghasilkan nilai maksimum apabila halaju cecair dangkal dan halaju gas dangkal berada pada tahap tertinggi. Konklusinya, projek ini menepati literatur sedia ada dan boleh ditambah baik untuk menentukan lokasi pengeringan dalam tiub menegak berdasarkan halaju sebenar buih.

ACKNOWLEDGEMENTS

First and foremost, I would like to extend my deepest gratitude to my almighty god, Allah S.W.T. for giving me a chance to complete this project as part of the graduation requirement for Master in Mechanical Engineering.

A special gratitude dedicated to my project supervisor, Dr. Mohd Zamri Bin Zainon, who gave me the opportunity to work on this project, educated me on the project related topics and provided constructive feedbacks during the writing of this report. I would also like to thank Mr. Mohd Asri Bin Ismail, the Thermal-hydraulics and Power Plant Laboratory assistant for his willingness to attend our experiment sessions to ensure we could complete all the tasks for the experiment. I am grateful for the help of Dr. Zamri’s ex-students and my fellow team members who ran the experiment with me.

Next, I would like to express my appreciation for my loving and patient husband, who has supported me throughout my final sprint of this Master program. Finally, I would like to thank my parents, siblings and friends who have directly and indirectly contributed to my mental well-being which allowed me to accomplish this feat.

TABLE OF CONTENTS

LIST OF FIGURES

LIST OF TABLES

LIST OF SYMBOLS AND ABBREVIATIONS

List of Symbols

A_L	:	Liquid phase cross-sectional area [m^2]
A_G	:	Gas phase cross-sectional area [m^2]
α	:	Void fraction [-]
m_G	:	Mass flow of gas [kg/s]
m_L	:	Mass flow of liquid [kg/s]
ρ_G	:	Density of gas [kg/ m^3]
ρ_L	:	Density of liquid [kg/ m^3]
υ_G	:	Mean velocity of gas [m/s]
υ_L	:	Mean velocity of liquid [m/s]
D_g	:	Diameter of channel occupied by gas [mm]
D_c	:	Diameter of channel [mm]
I_O	:	Constant current
R_{TP}	:	Resistance of two-phase flow
R_{SP}	:	Resistance of single-phase liquid flow
S	:	Slip ratio [-]
j_G	:	Gas superficial velocity [m/s]
j_L	:	Liquid superficial velocity [m/s]
υ_b	:	Bubble actual velocity [m/s]
Q_G	:	Gas volumetric flow rate [LPM]
L/D	:	Axial position [-]
V_x	:	Voltage reading (x = 1, 2, 3,4 and 5) [V]

List of Abbreviations

ECCS	:	Emergency Core Cooling System
PWR	:	Pressurized Water Reactor
DCC	:	Direct Contact Condensation
LOCA	:	Lost of Coolant Accident
CECM	:	Constant Electric Current Method
NI	:	National Instrument®
DAQ	:	Data Acquisition
LabVIEW®	:	Laboratory Virtual Instrument Engineering Workbench
PDF		Probability Density Function
PSD		Power Spectral Density
EE		Eularian-Eularian
LE	:	Lagrangian-Eularian
NR	:	Neutron Radiography
NMR	:	Nuclear Magnetic Resonance

LIST OF APPENDICES

CHAPTER 1: INTRODUCTION

1.1 Introduction

1.1.1 Background

In the energy industry, two-phase flow is the most common type of flow, particularly when steam is required as a working fluid such as in power generation or applied as a medium for refinery processes. Simultaneous flow of steam and liquid water requires adequate piping design to meet process specifications. Various studies have been done on two-phase flow, particularly for flow patterns which also include investigations on the structures and mechanisms of their dynamics behaviors such as the volumetric flow rate or called the void fraction, film thickness and other governing parameters.

1.1.2 Application of Two-Phase Flow in Nuclear Power Plants

Among many industrial applications, two-phase flow is common in nuclear and thermal plants. Although each nuclear plants are designed differently, a reactor cooling system is a necessary component of the design. Two-phase flow exists in the Emergency Core Cooling System (ECCS) of a Pressurized Water Reactor (PWR). In the pressurizer component of a PWR, it is important to maintain the coolant at optimal temperature and pressure to avoid boiling. According to Pressure Law, in a fixed volume, pressure and temperature are directly proportional. Hence, if pressure increase in the pressurizer, so does the temperature. In order to avoid boiling occurrence in the coolant, a Direct Contact Condensation (DCC) technique is used, where high temperature steam is sprayed into the wet-well suppression pool to control the pressure in the pressurizer. The behavior of two-phase flow such as the flow pattern and void fraction are important parameters to be determined to avoid unstable and abrupt pressure change which could lead to catastrophic incidents such as the Fukushima Disaster in 2011.

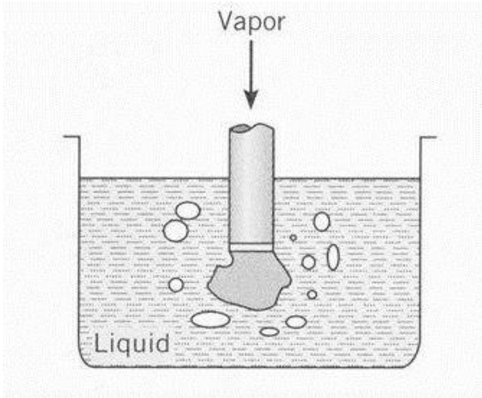

Figure 1.1: Direct contact condensation application where vapor is injected into cooling liquid (Incropera, 2006).

1.2 Problem Statement

While many argued that the Fukushima Daiichi incident was caused by natural disasters, earthquake and tsunami that followed after, the nuclear reactors explosions could have been prevented if the cooling system in the reactors were more efficient. This specific problem is called the Loss of Coolant Accident (LOCA). Due to power outage when tsunami waves hit the nuclear plant, the cooling system could not function optimally as there were no electricity to drive the turbine generators that were used to recirculate water in the cooling system. With the determination to prevent such incident from happening, there have been many works carried out since the 1950's (Wallis, 1969) which purpose is also to further improve the cooling system of a reactor. One of the most important factors affecting the piping design for better cooling efficiency is the volumetric flow rate, also known as void fraction, calculation. As LOCA could have been prevented if the cooling system is more efficient, it is therefore very important to study and to improve the design of a piping systems to allow efficient cooling to take place.

1.3 Research Aim and Objectives

Utilizing an industrial scale of a two-phase flow rig at the Thermal-hydraulics and Power Plant Laboratory, Department of Mechanical Engineering, University of Malaya, a series of experimentations were conducted to study the flow pattern resulted from varying gas and liquid flowrates in the co-current two-phase flow. Therefore, the objectives of this research experiment are as follows:

I. To study the flow pattern behavior in a vertical channel during a gas-liquid co-current flow; and

II. To measure the void fraction using Constant Electric Current Method (CECM); and

III. To compute actual bubble velocity along two-phase flow at different gas and liquid flowrates by utilizing void fraction results.

Thorough investigation into these 3 objectives could help in the optimal design of vertical DCC condenser.

1.4 Research Scope

In order to obtain a reliable and accurate results to meet the objectives of this work, experiments were conducted under steady state and atmospheric condition with the following procedures and assumptions:

I. Air bubbles were released from the bottom of the flow channel to replicate the steam generation from boiling and hence it is easier to control the flow condition without temperature effects.

II. Both air and water superficial velocity were controlled via flow meters and their fraction were characterized as the slip ratio in order to meet the high temperature boiling requirement.

III. Flow structures and dynamic changes of the two-phase flow were investigated using a 3-m vertical flow channel, installed with void meter for data recording.

IV. Sophisticated data collections were performed using reliable tools such as National Instrument® (NI) data acquisition and LabVIEW® software.

V. All the numerical data were translated into graphic presentation and discussed in Chapter 4.

CHAPTER 2: LITERATURE REVIEW

2.1 Two-phase Flow

2.1.1 Introduction

Multiphase flow occurs when two or more phases with distinctive properties flow simultaneously, such as when different state of matters, namely, gas, liquid and solid interact in a flow. Aside from the state of matter, a multiphase flow can also be an interaction between chemical with different properties in the same state, but they are most unlikely categorized in this manner even though they coexist and blend easily. Two-phase flow is the most and encountered extensively in energy-related or process industries. Phase combinations for two-phase flow could be solid-liquid combination, solid-gas combination, liquid-gas combination and all states combination (Faghri et al., 2006). However, the combination of gas-liquid or vapor-liquid are mostly studied compared to the rest due to the widely used application in the industry.

2.1.2 Flow Patterns in Vertical Tubes

Two-phase flow in vertical tubes is symmetric due to the nature of gravity where all gravitational forces is the equal around the tube circumference. According to Holland et al. (1995), flow patterns in vertical tubes are classified into five categories, bubbly flow, slug flow, churn flow, wispy-annular flow and annular flow. In ascending order, as the ratio of gas flow rate to liquid flow rate increases, the flow develop into an annular flow where a liquid layer is formed on the pipe wall while gas flow through the center of the tube.

2.1.2.1 Bubbly Flow

A bubbly flow consists of gas bubbles at different sizes distributed along the liquid. As gas flow rate is lower compared to liquid flow rate, most of the gas bubbles disperses in the liquid flow.

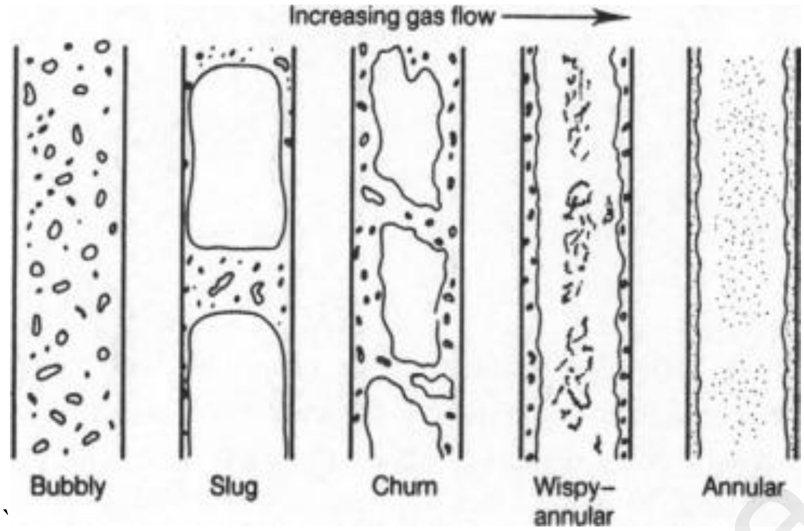

Figure 2.1: Flow Patterns in Vertical Tubes in Increasing Gas Flow Rate (Holland et al., 1995).

2.1.2.2 Slug Flow

With higher gas flow rate, bubble size increases which causes the small bubbles to coalesce, forming a ‘slug’. In a vertical upward flow, these slugs are often bullet-shaped and takes up the cross-section of the tube, separated from the wall by thin liquid film.

2.1.2.3 Churn Flow

Churn flow, also known as semi-annular flow, represents an oscillatory pattern where the liquid flows upward and also downward when the bubbles become larger. As the slug bubbles become larger, they also start to break up which causes the flow to be more unstable. Typically, churn flow is avoided, due to its unstable nature, by having smaller vertical tube.

2.1.2.4 Wispy-annular Flow

An increase in gas flow rate would lead to phases separation where thin liquid layer would form along the walls of the tube. However, at high liquid flow rate, more liquid droplets would form in the middle of the tube which is occupied by vapors. The liquid droplets combine and form ‘wisps’ of liquid.

2.1.2.5 Annular Flow

The difference between annular flow and wispy annular flow is that further increase in the gas flow rate would result in the vapor shear force along liquid film to be more dominant over gravity. This would cause the vapor core to push the liquid layer from the core towards the thin liquid film at the tube wall.

2.1.3 Flow Regime Map

Flow regime maps are inferred from experimental reflectivity which determines the interfacial structure and area, supported by theoretical basis. Hewitt and Roberts (1969) developed a flow regime map for vertical upward two-phase flow where the relationship between volumetric fluxes of liquid and gas are compared.

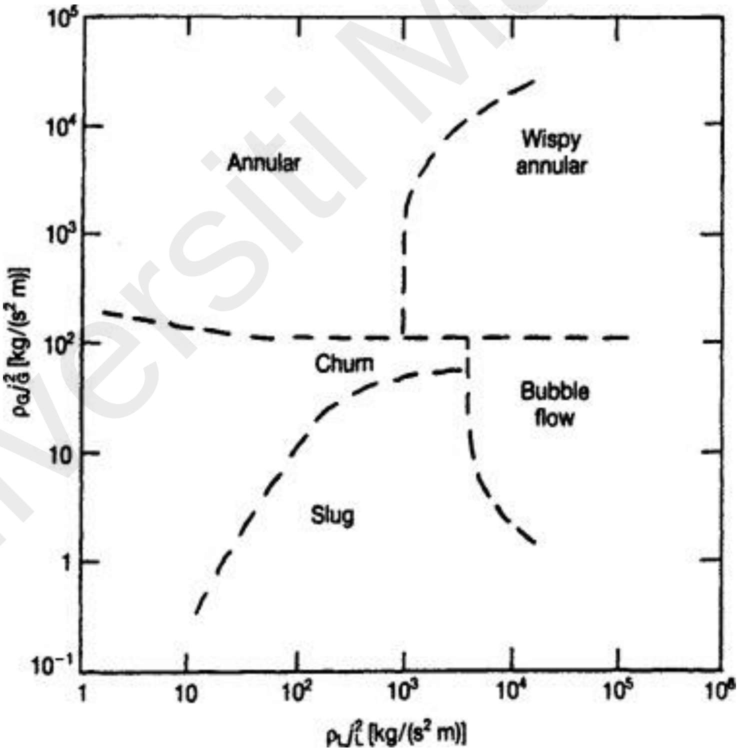

Figure 2.2: Flow regime map for vertical upward two-phase flow (Hewitt and Roberts, 1969).

From Figure 2.2, the y-axis represents the volumetric flux of the gas while x-axis represents the volumetric flux of the liquid. To calculate the volumetric flux, the volumetric flow rate of the gas or liquid is divided by the cross-sectional area of the pipe.

The flow regime map displays the relationship of gas and liquid flow rates with the change in flow patterns. Hewitt and Roberts (1969) produced the flow regime map by varying the gas and liquid momentum flux, either by increasing it or decreasing it.

2.1.4 Flow Patterns Identification Method

There are a few methods that can be used to identify the flow patterns which are by measuring void fraction, by using the probability density function (PDF) technique, by using power spectral density (PSD) analysis and by using tomographic imaging method.

2.1.4.1 Probability Density Function Method

As the name suggest, probability density function relies on the probability distribution of the flow pattern variable. According to Pai (2007), PDF method that is represented using statistical formalism can be categorized into Eularian-Eularian (EE) and Lagrangian-Eularian (LE). Since two-phase flow behavior is affected by multiple variables, a statistical approach could not be avoided to achieve reliable results. However, both statistical representation requires more time and effort to create the model that yields acceptable results.

2.1.4.2 Power Spectral Density Method

Power spectral density measures power signal of an equipment and compare it to the equipment frequency. It is usually used together with the probability density function method when measuring a specific random process (Slavic et al., 2021). Although PSD method is reliable, easily computed and inferred, the frequency coverage is limited and the assumption of the signal remaining static is not very accurate for a multiphase flow (Luo et al., 2006).

2.1.4.3 Tomographic Imaging Method

Tomographic imaging techniques were adopted from medical practices such as X-ray tomography, MRI, PET and also gamma-ray tomography (Hampel et al., 2020). This method is used to identify and analyze the flow patterns in tubes by using a cone-beam tomography paired with a rotating scanning system. This method is highly used for nuclear safety research but would require a large capital to set up the research facility.

2.2 Void Fraction

2.2.1 Introduction

Void fraction, denoted as, α, is an important parameter that is used to observe and analyze two-phase flow. It represents the ratio between gas phase area and total geometric area at a cross-section, affecting the characteristic behavior of a flow such as flow pattern, viscosity, pressure drop and heat transfer coefficient. Void fraction can be numerically presented between 0 to 1, where 0 indicates that the flow is fully-liquid while 1 indicates that the flow is fully occupied with gas. Aside from channel cross-sectional area, void fraction could also be represented in a volume of a channel. Volumetric void fraction represents the ratio of a channel volume gas phase and total geometric volume. A_g denotes the gas phase area while A_L denotes liquid phase area.

$$\alpha = \frac{A_g}{A_g + A_L} \tag{1}$$

2.2.2 Void Fraction Measurement Methods

Several methods have been developed to measure void fraction for two-phase flow along a channel. There are the quick shut valve method, probe method, image processing method, X-ray CT scan method, neutron radiography (NR) method, gamma-ray method, nuclear magnetic resonance (NMR) method and electromagnetic-conductance method. However, according to Uesawa et al. (2012), X-ray CT scan methods, NR methods, gamma-ray methods and NMR would require a large amount of financial spending to build a working facility and need longer time to obtain the void fraction data. Although the quick shut valve and probe methods are simple and accurate for average void fraction results, these methods cause non-continuous flow which would change the channel properties and gives inaccurate results (Chang et al., 2020). Based on the study of Chang et al. (2020) on electromagnetic-conductance method, the method has not been tested for the accuracy to measure void fraction in vertical channels, which are typically used for industrial application.

2.3 Constant Electric Current Method to Measure Void Fraction

2.3.1 A Brief Overview

Constant Electric Current Method (CECM) was developed by Fukano (1998) where electrical power is supplied through two electrodes with constant-current along the flow. It was specifically used to measure liquid films with high-speed gas flow behavior involving the flow pattern, liquid film thickness and interfacial stress. From Figure 2.3, the basic set up of equipment to use the CECM for flow pattern analysis would be to have two power electrodes and as many sensor electrodes at each measuring point. High input impedance amplifier exists to read the voltage drop across the flow at each sensor electrodes where resistance is higher due to presence of gas bubbles. This method is highly accurate as the sensor electrodes measures the electrical resistance of each gas phase regardless of the bubbles' location along the cross-sectional area passing through the electrodes (Fukano, 1998).

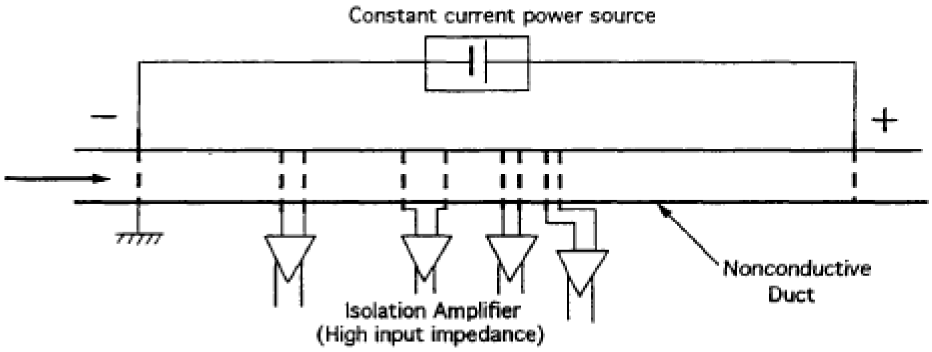

Figure 2.3: Basic Schematic for Constant Electric Current Method (Fukano, 1998).

2.3.2 Mathematical Model and Equations

To measure void fraction using constant electric current method, a basic equipment configuration in Figure 2.4 is referred. The power electrodes should be placed further from the sensor electrodes to avoid any reading disturbances (Fukano, 1998).

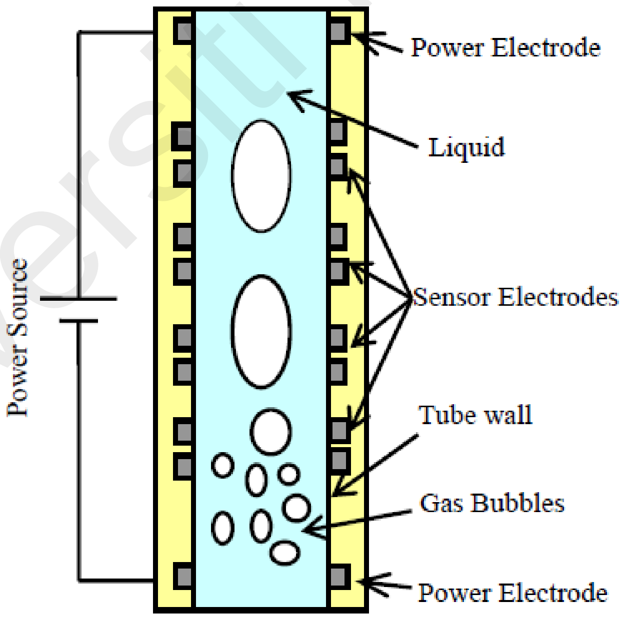

Figure 2.4: Configuration of CECM Sensors (Zainon, 2014).

Assuming an adiabatic vertical upward flow with constant liquid mass flow, m_L, and density, ρ_L, together with constant gas mass flow, m_G, and density, ρ_G, void fraction could be measured by the following equations.

$$\alpha = \frac{A_g}{A_C} = \frac{1}{1 + \frac{m_L \rho_G v_G}{m_G \rho_L v_L}} \tag{2}$$

Where A_C also denoted the addition of gas phase area to liquid phase area. υ_G and υ_L are the gas mean velocity and liquid mean velocity respectively. A simplified equation is represented in Equation 3.

$$\alpha = \frac{A_g}{A_C} = (\frac{D_g}{D_C})^2 \tag{3}$$

On the other hand, the fraction for liquid hold up can be expressed as,

$$\eta = 1 - \alpha = 1 - \left(\frac{D_g}{D_C}\right)^2 \tag{4}$$

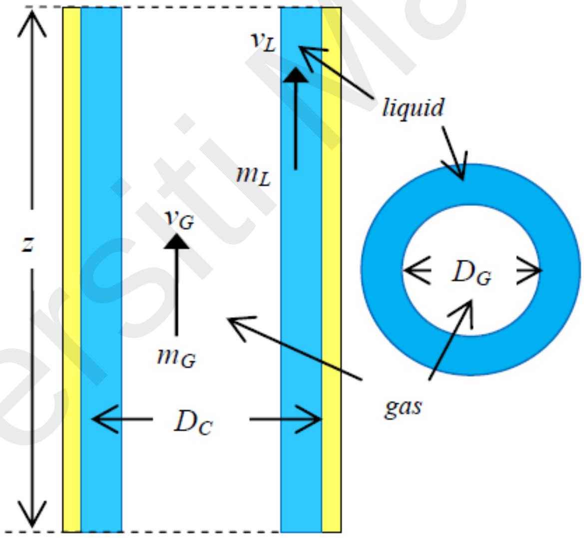

Figure 2.5: Void Fraction Model Depiction (Zainon, 2014).

2.4 Instantaneous Bubble Velocity

Since the gas flow inside the tube is only defined as superficial velocity which is the flux of the gas flowing in a channel under a substance with higher density (water, in this experiment), the actual bubble velocity is therefore not accurately determined. Actual bubble velocity, or normally termed as instantaneous bubble velocity, is very important to be calculated since it determines the location of dryout or burnout occurrent in a heated channel. Burnout phenomenon occurs when the cooling liquid could not withstand the vapor high temperature which causes the channel wall to absorb the heat. This could result in the melting of the channel and disastrous effect such as LOCA.

2.5 Outcome of Literature Review

As two-phase flow is widely used in the industry, many studies have been conducted to develop optimal piping designs for the intended processes. Specifically to two-phase flow involving gas and liquid phases, the flow patterns will develop from bubbly flow to slug flow, slug flow into churn flow, churn flow into wispy-annular flow and finally into annular flow. Aside from the flow pattern behavior, cooling system design can be improved by calculating the void fraction in the channel. Void fraction measurement using the constant electric current method (CECM) has been proven reliable and accurate by other literatures while also being cheap and simple. In addition, by utilizing the void fraction measurement, instantaneous bubble velocity along the channel can be calculated. There have not been many literatures measuring the actual bubble velocity for a two-phase flow in a vertical channel experiment. It is important to calculate the actual bubble velocity to determine the dryout location in a heated channel since dryout occurrence could result in loss of coolant (LOCA) disaster.

CHAPTER 3: METHODOLOGY

3.1 Introduction

As discussed in previous chapter, two-phase flows are common in many industrial applications especially involving gas-liquid flow. It is a challenging topic as the flow pattern behavior along the channel changes with different condition, hence, research must be conducted to achieve optimal design. To provide clarity, this chapter will discuss thoroughly theoretical and experimental methods used for data collection. Two-phase flow experimental rig was developed previously at the Thermal-hydraulics and Power Plant Laboratory, University of Malaya, to carry out the experiment with varieties of gas and liquid flow conditions.

3.2 Two-Phase Flow Experimental Rig

Figure 3.1 represents the schematic drawing of the experimental rig utilized for this work. Based on the apparatus set-up, the flow patterns, average void fractions and gas bubble velocities can be determined at different gas and liquid flowrates.

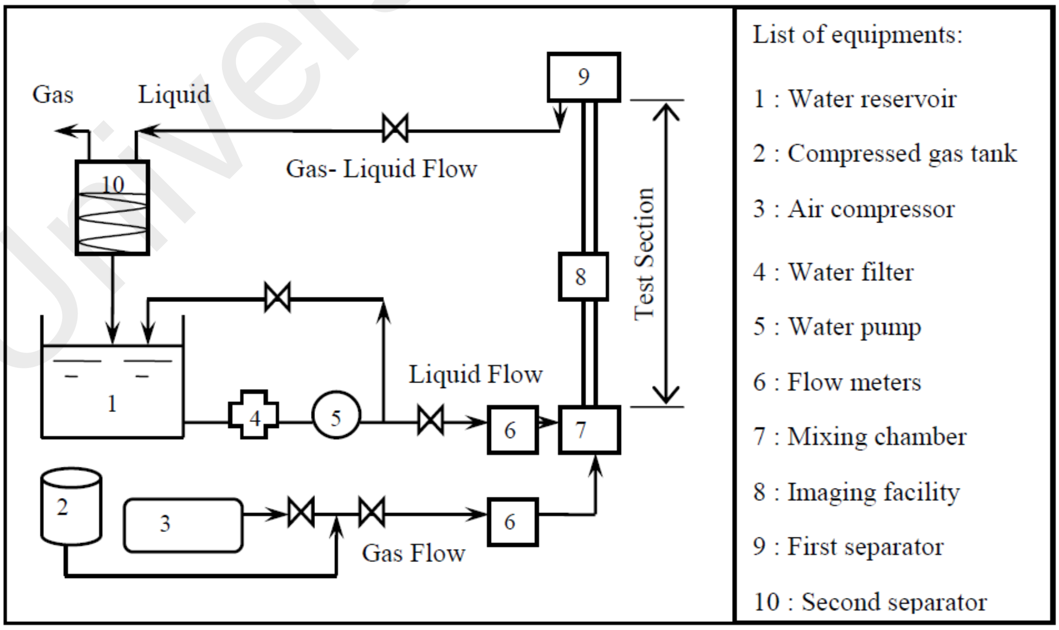

Figure 3.1: Two-Phase Flow Experimental Rig (Zainon et al., 2014).

Zainon et al. (2014), Zuber et al. (2019) and Ismail (2020) had also used the exact experimental rig set-up to study the two-phase flow behaviors in a vertical channel such as the flow patterns, flow mappings, void fraction measurements and liquid film thickness. Therefore, it is suitable to assume that the experimental rig could present relevant and reliable outputs.

The actual experimental rig is shown in Figure 3.2. A 40-mm diameter transparent acrylic tubes serve as the channel flow which goes up to 3.8-m height. Two power electrodes were installed at the top and bottom of the channel while five sensor electrodes to measure the voltage drop across the channel were installed at 0.6-m intervals. The temperature along the channel was maintained at 27-30°C throughout the experiment.

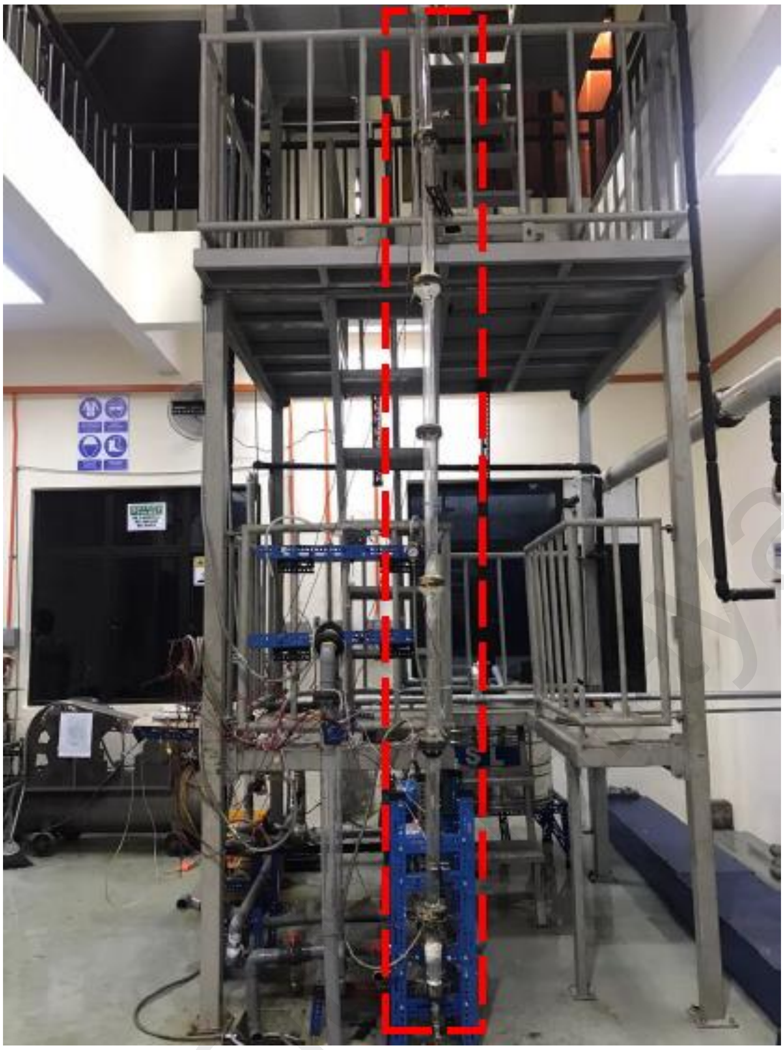

Figure 3.2: Actual Experimental Rig Thermal-hydraulics Laboratory, University of Malaya.

Water was supplied through PVC piping into the bottom of the channel using 3kW Ebara (Japan) water pump, connected to a water tank. The water was controlled by the Blue-White® (USA) flow meter, which was pre-calibrated manually using a stopwatch to measure the time taken for the water to travel between two sensor electrodes. In order to create a two-phase flow, air from an air compressor was supplied through a welded fitting at the bottom of the channel which is shown in Figure 3.3. The gas flowrate was measured using a Kofloc® (Japan) air flowmeter. The two-phase flow travelling through the channel flowed into a separator at the top of the channel and water was recirculated into the water tank.

Figure 3.3: Welded Fitting to Inject Air.

3.2.1 Construction of Constant Electric Current Method (CECM)

As discussed earlier in section 2.3, the constant electric current method requires two power electrodes at the end of each channel sides to supply constant current and several pairs of sensor electrodes to measure voltage across each point identified along the channel. The voltage will increase during the two-phase flow when gas bubbles pass through the sensor electrodes where void fraction can be calculated.

When constant current I_O is applied, the resistance of two-phase flow, R_{TP}, will be higher than the resistance of single-phase liquid flow, R_{SP}. According to Ohm's Law, the resulting voltages for two-phase flow and single-phase flow would be directly proportional to the resistance values which will be V_{TP} and V_{SP} respectively. The hold-up value, η, which is the amount of liquid in the channel, as also discussed in section 2.3 (Equation 4), can be calculated from Equation 5.

$$\eta = \frac{R_{SP}}{R_{TP}} = \frac{I_O R_{SP}}{I_O R_{TP}} = \frac{V_{SP}}{V_{TP}} \quad (5)$$

In more definitive description, when $\eta=1$, the flow channel would be filled entirely with liquid, and when $0<\eta<1$, would mean the existence of gas bubbles together with the liquid in the flow channel. Therefore, by applying the CECM sensor, the void fraction can be calculated using the following equation,

$$\alpha = 1 - \eta = 1 - \frac{V_{SP}}{V_{TP}} \tag{6}$$

3.2.2 Slip Ratio

Another important parameter to measure void fraction for a two-phase flow is the slip ratio. According to Butterworth (1975), void fraction and slip ratio are directly proportional to each other. Slip ratio, S,can be calculated by dividing superficial gas velocity, j_G, to superficial liquid velocity, j_L, represented in Equation 7.

$$S = \frac{j_G}{j_L} \tag{7}$$

3.2.3 Actual Bubble Velocity

Based on the void fraction result generated by LabVIEW®, the actual bubble velocity could be inferred. Using Equation 8, the bubble velocity could be calculated as the length and time taken for the bubble to travel the distance are known.

$$v_b = \frac{l}{t} \tag{8}$$

3.2.4 Experimental Equipment and Apparatus

3.2.4.1 Water Pump

The experimental facility includes an Ebara type DWO 400 model water pump with 4-hp equivalent to 3-kW power source and 3-phase induction motor of 240V, 50Hz, 10A.

Figure 3.4: Water Pump.

3.2.4.2 Acrylic Tube

Acrylic tubes were used as it is transparent which makes it suitable for flow pattern observation. It has an inner diameter of 40-mm, an outer diameter of 50-mm and is 3-m in length. Compressed air was supplied from a 2-kW air compressor through a copper nozzle with inner diameter of 2-mm submerged at the bottom of the flow channel.

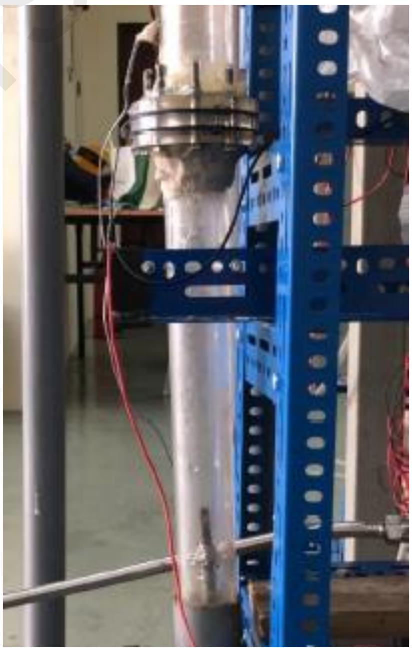

Figure 3.5: Acrylic Tube.

3.2.4.3 Water Tank

A 500-L capacity water tank was used for the water circulation in the research facility. It is made out of stainless steel to prevent from corrosion and rust.

Figure 3.6: Water Tank.

3.2.4.4 Gas-Liquid Separator

The separator is located at the top of the experimental rig which function is to separate air and water. The air was released into the atmosphere while the water is recirculated into the water tank. By having a separator, over-pressure which can cause backflow along the acrylic tubes can be avoided.

Figure 3.7: Gas-Liquid Separator.

3.2.4.5 Power and Sensor Electrodes

3.2.4.6 Data Acquisition (DAQ)

To connect the sensors to the LabVIEW® software, a National Instrument® data acquisition system, NI USB-6215 was utilized. It has 16 analog inputs, 2 analog outputs, 4 digital inputs and 2 32-bit counters. The device was designed to receive 10V voltage and could transform the data collected into numerical values and graphical interface through LabVIEW® software.

3.2.4.7 Direct Current Supply (DC)

For a constant electric current, the Gardner-Well® power generator, GW GPS303D, was used to supply 3A current through the power electrodes installed at top and bottom of the acrylic tubes.

3.2.5 Experimental Set-Up

3.2.5.1 Schematic Diagram

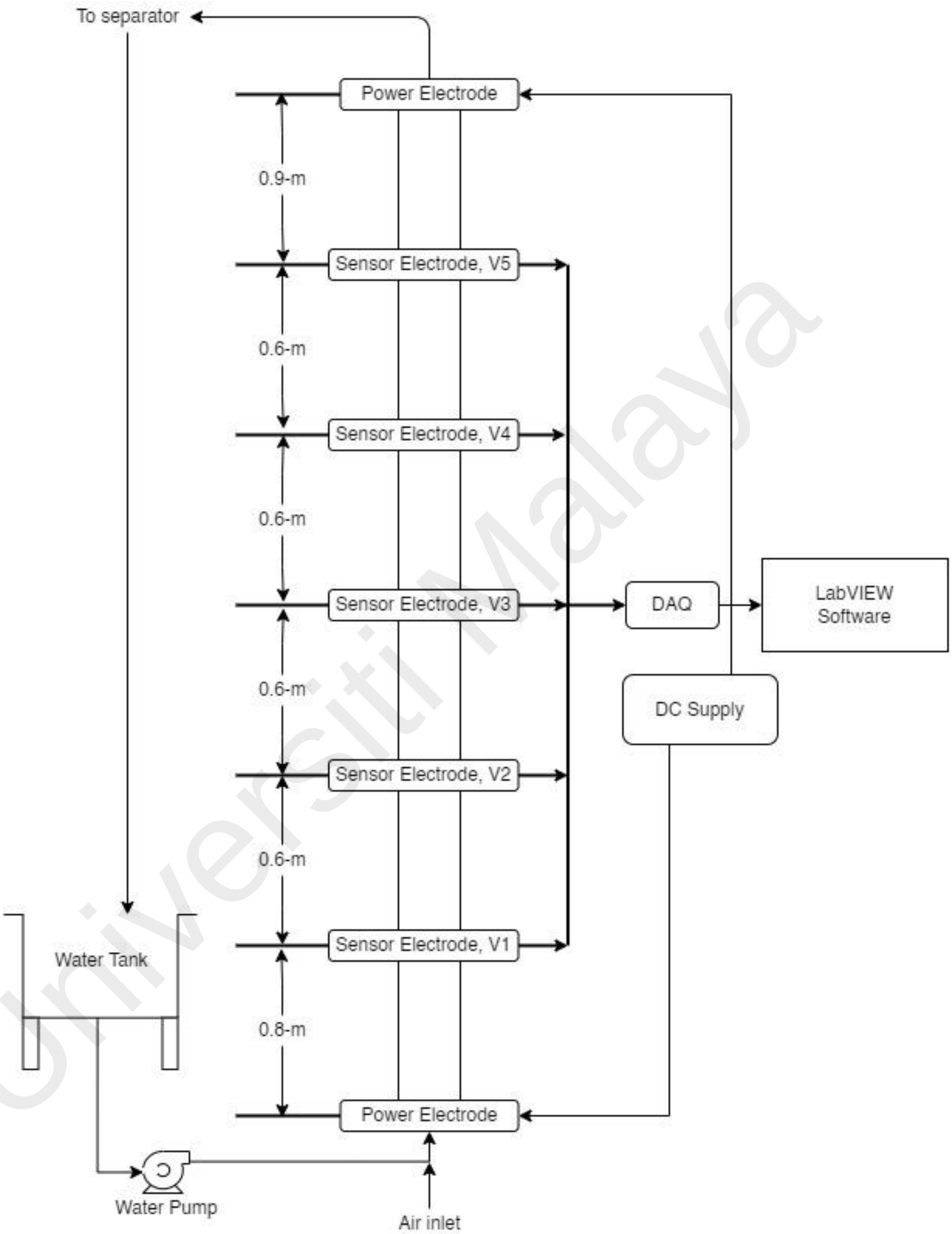

Figure 3.8: Schematic Diagram of Experimental Rig.

3.2.5.2 Data Collection and Interpretation

In the LabVIEW® software, a block diagram was designed to collect and analyze data output from sensor electrodes. The block diagram was developed using LabVIEW® built in functions. Meanwhile, the data collected and analyzed result were tabulated in the form of waveform graph and numerical display in the front panel interface. There is also an excel file that stores the data which was captured according to LabVIEW® manual setting which was set for capturing 10,000 data in 10 seconds.

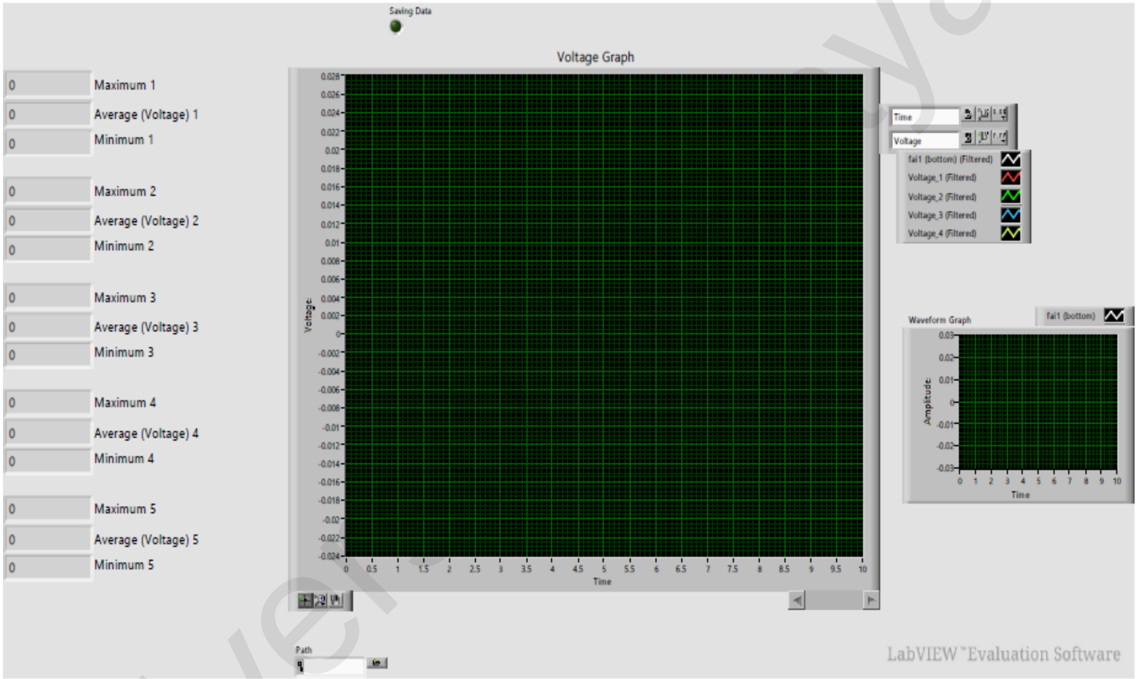

Figure 3.9: LabVIEW® Front Panel Interface.

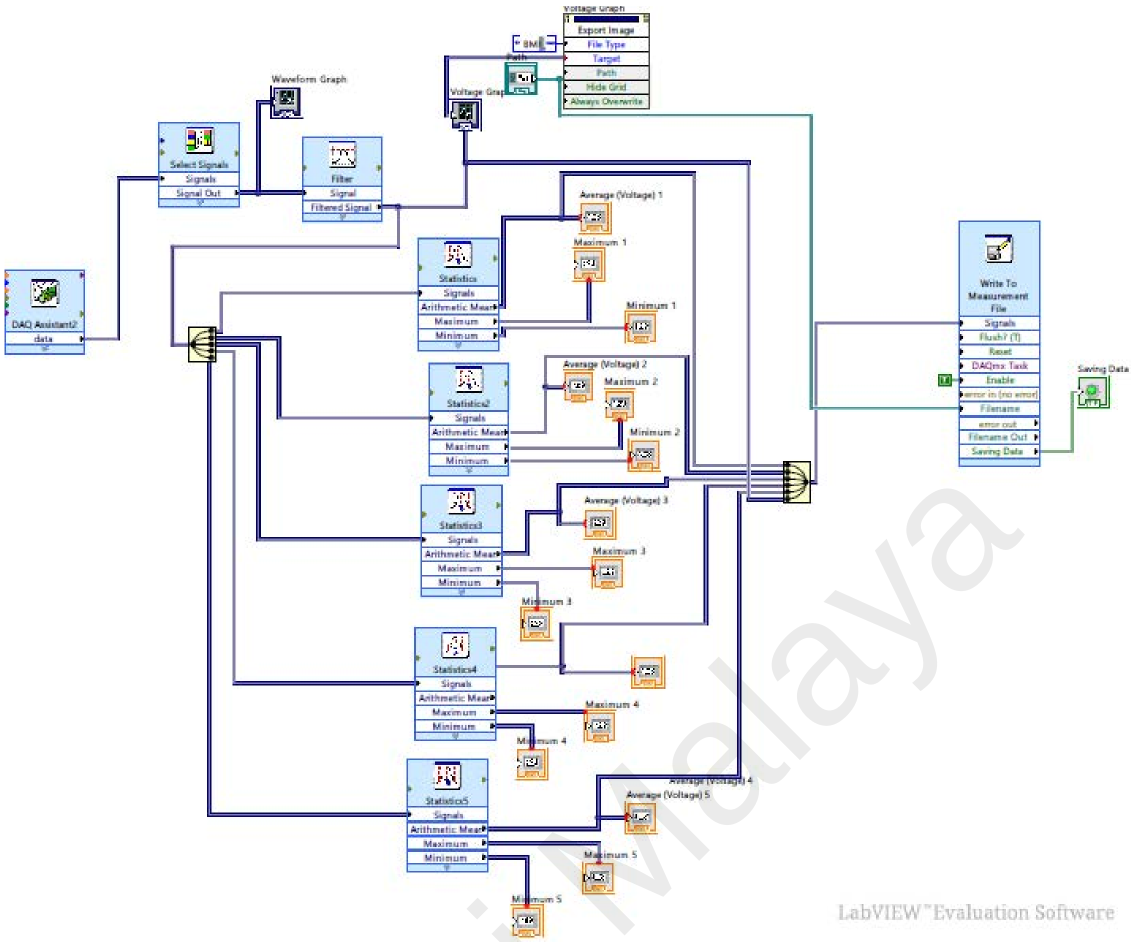

Figure 3.10: LabVIEW® Block Diagram Interface.

3.3 Experimental Procedures

The flow conditions for this experiment are based on combination of different liquid and gas superficial velocities (j_L and j_G). Three different liquid superficial velocities, j_L, set at 0.071-m/s, 0.227-m/s and 0.397-m/s, and gas volumetric flow rates will be varied between 2-L/min to 30-L/min which represent gas superficial velocity, j_G, of 0.0265-m/s to 0.3979-m/s. The voltage fluctuations at each sensor electrodes will be analyzed to determine the void fraction profiles and will be used to calculate actual gas bubble velocity. Figure 3.11 represents the experimental procedures for this study.

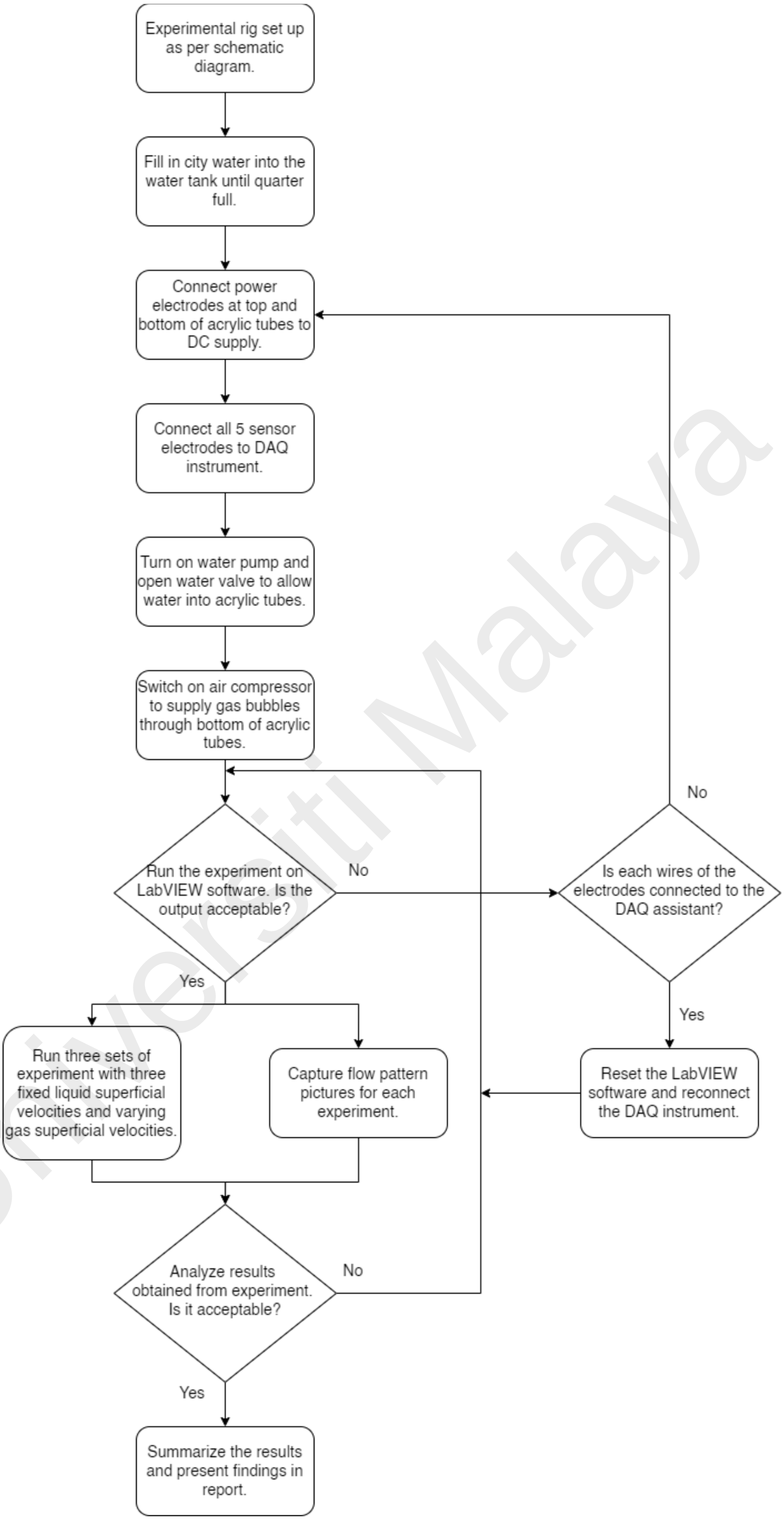

Figure 3.11: Experimental Procedure Flow Chart.

CHAPTER 4: RESULTS AND DISCUSSIONS

4.1 Introduction

Vertical co-current two-phase flow study is very important as it is used in many engineering applications especially in thermal plants involving gas-liquid flow. Based on the study objectives, a series of experimentations have been conducted by varying gas and liquid flow rates with similar working condition. The purposes of these experiments were to observe the flow patterns and to record the void fraction profiles along the test channel, which the latter is used to calculate the actual bubble velocity.

4.2 Experimental Data

The experiments were carried out by varying 3 sets of combination of flow condition as listed in section 4.1. Table 4.1 shows the gas flow rate at which each set of experiment were carried out. In order to assign the gas superficial velocity, volumetric flow rate, which was measured using a Kofloc® (Japan) air flowmeter, is divided by the cross-sectional area of the tubes as the following relationship.

$$j = \frac{Q}{A} \ [\mathrm{m/s}] \qquad (9)$$

Table 4.1: Gas Flow Rate

Gas Volumetric Flow Rate, Q_G		Tube Cross-sectional Area	Gas Superficial Velocity, j_G
[L/min]	[m^3/s]	[m^2]	[m/s]
2.0	0.000033	0.0012566	0.0265
3.0	0.000050		0.0398
5.0	0.000083		0.0663
7.5	0.000125		0.0995
10.0	0.000167		0.1326
12.5	0.000208		0.1658
15.0	0.000250		0.1989
17.5	0.000292		0.2321
20.0	0.000333		0.2653
25.0	0.000417		0.3316
30.0	0.000500		0.3979

For each experiment, while the liquid superficial velocity is kept constant, the gas superficial velocity is changed to observe the flow patterns. Table 4.3 represents the voltages reading recorded at each sensor electrodes, placed at distances L_x from the gas injection point, where x is numbered from 1 to 5 representing the section of the test channel which is divided by the locations of sensor electrodes. The axial locations of the sensors are the distance, L_x, to diameter ratio of the vertical pipe, L_x/D. Figures 4.1, 4.2 and 4.3 are the voltage readings plotted at each sensor electrodes for experiment with liquid superficial velocity, j_L, at 0.071-m/s, 0.227-m/s and 0.397-m/s respectively. The voltage results were computed as an average value of data taken within 10 seconds.

Table 4.2: Experimental Voltage Results

Liquid Superficial Velocity, j_L	Gas Superficial Velocity, j_G	Voltage Electrode 1, V_1 L/D = 20	Voltage Electrode 1, V_2 L/D = 35	Voltage Electrode 1, V_3 L/D = 50	Voltage Electrode 1, V_4 L/D = 65	Voltage Electrode 1, V_5 L/D = 80
[m/s]	[m/s]	[V]	[V]	[V]	[V]	[V]
0.071	0	0.0086	0.0257	0.0327	0.0048	0.0034
	0.0265	0.0028	0.0225	0.0328	0.0025	0.0009
	0.0398	0.0004	0.0203	0.0319	0.0016	0.0024
	0.0663	0.0022	0.0183	0.0313	0.0001	0.0046
	0.0995	0.0051	0.0156	0.0310	0.0011	0.0068
	0.1326	0.0067	0.0142	0.0300	0.0026	0.0087
	0.1658	0.0118	0.0094	0.0268	0.0067	0.0130
	0.1989	0.0105	0.0098	0.0271	0.0062	0.0131
	0.2321	0.0111	0.0096	0.0270	0.0061	0.0135
	0.2653	0.0111	0.0095	0.0274	0.0062	0.0137
	0.3316	0.0120	0.0090	0.0269	0.0066	0.0143
	0.3979	0.0130	0.0070	0.0264	0.0074	0.0156
0.227	0	0.0033	0.0173	0.0189	0.0004	0.0014
	0.0265	0.0047	0.0116	0.0225	0.0031	0.0062
	0.0398	0.0066	0.0089	0.0215	0.0036	0.0073
	0.0663	0.0097	0.0068	0.0209	0.0049	0.0100
	0.0995	0.0118	0.0045	0.0191	0.0063	0.0122
	0.1326	0.0122	0.0037	0.0189	0.0072	0.0134
	0.1658	0.0138	0.0027	0.0193	0.0074	0.0138
	0.1989	0.0157	0.0019	0.0175	0.0084	0.0148
	0.2321	0.0169	0.0014	0.0186	0.0086	0.0157
	0.2653	0.0175	0.0006	0.0190	0.0090	0.0167
	0.3316	0.0183	0.0006	0.0183	0.0095	0.0166
	0.3979	0.0186	0.0011	0.0182	0.0099	0.0176
0.397	0	0.0415	0.0198	0.0254	0.0269	0.0523
	0.0265	0.0433	0.0095	0.0093	0.0211	0.0421
	0.0398	0.0461	0.0139	0.0067	0.0237	0.0450
	0.0663	0.0441	0.0149	0.0076	0.0244	0.0448
	0.0995	0.0468	0.0178	0.0085	0.0257	0.0470
	0.1326	0.0483	0.0206	0.0073	0.0266	0.0489
	0.1658	0.0469	0.0226	0.0068	0.0256	0.0445
	0.1989	0.0455	0.0219	0.0052	0.0274	0.0478
	0.2321	0.0380	0.0172	0.0036	0.0198	0.0326
	0.2653	0.0386	0.0205	0.0020	0.0190	0.0325
	0.3316	0.0378	0.0184	0.0035	0.0213	0.0318
	0.3979	0.0376	0.0161	0.0021	0.0202	0.0336

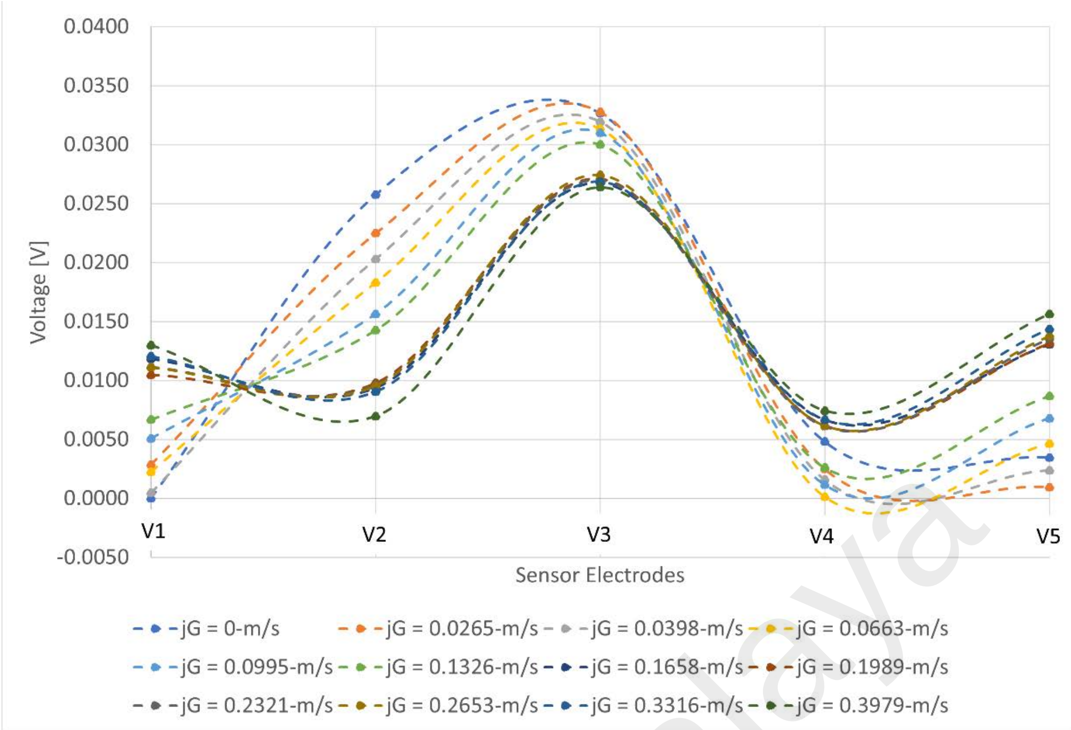

Figure 4.1: Voltage Readings at Each Sensor Electrodes With Constant Liquid Superficial Velocity, j_L = 0.071-m/s.

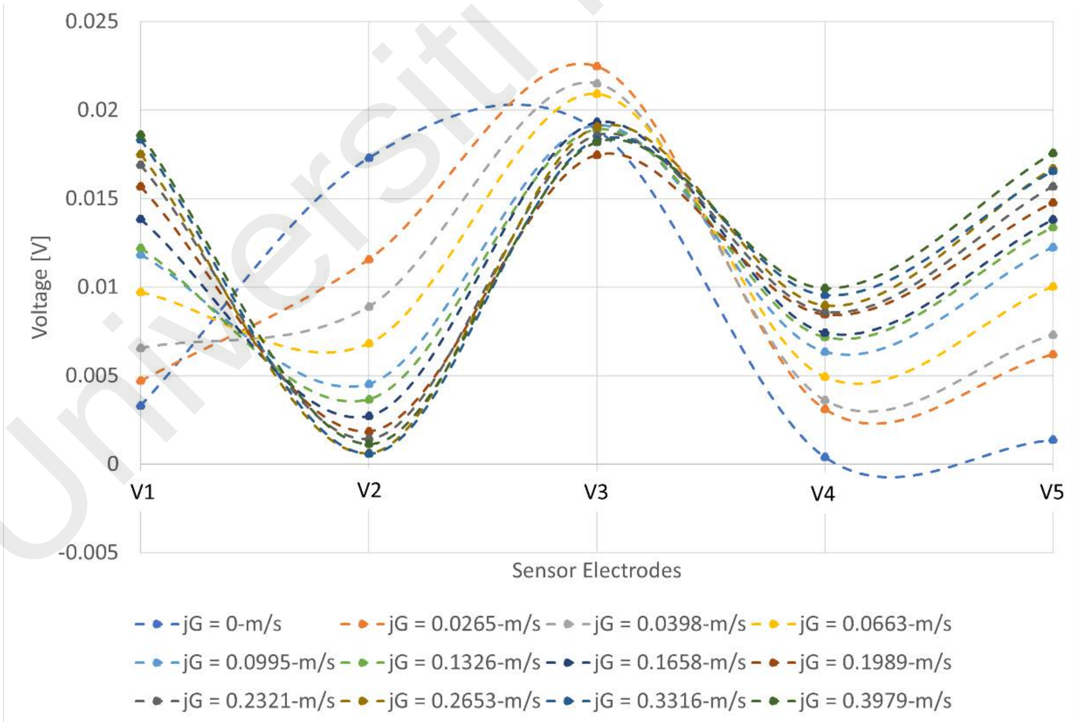

Figure 4.2: Voltage Readings at Each Sensor Electrodes With Constant Liquid Superficial Velocity, j_L = 0.227-m/s.

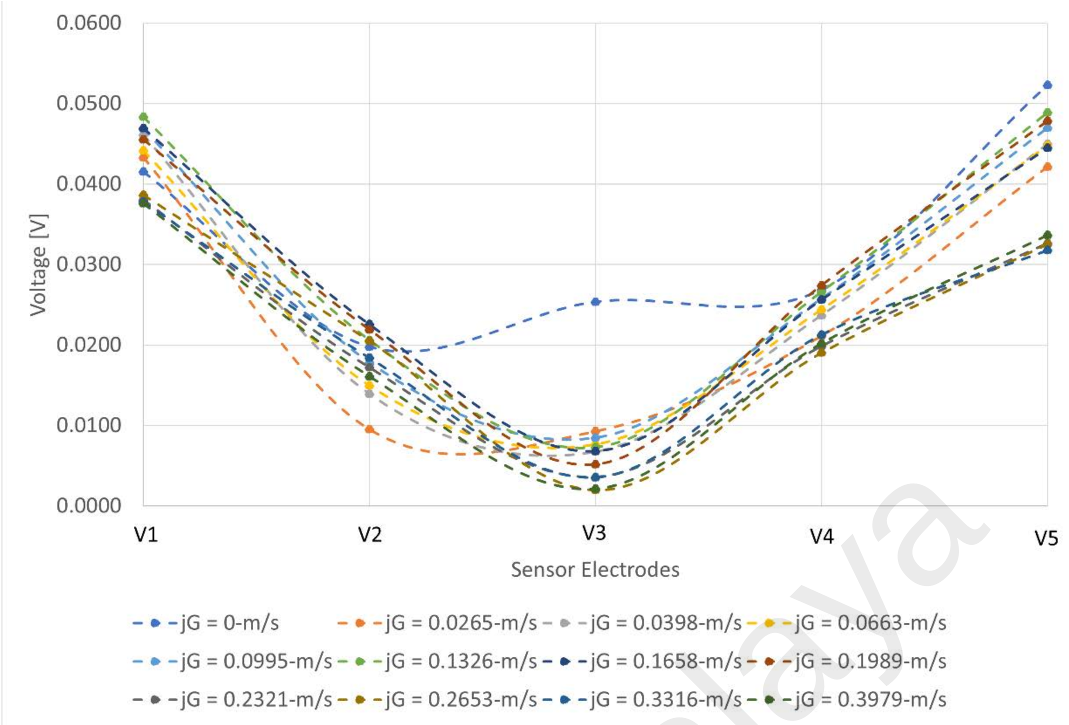

Figure 4.3: Voltage Readings at Each Sensor Electrodes With Constant Liquid Superficial Velocity, j_L = 0.397-m/s.

Based on the figures 4.1 ~ 4.3, the voltage readings with liquid superficial velocity j_L = 0.071-m/s and j_L = 0.227-m/s show similar trends. The voltage reading is highest at sensor electrode 3 which indicates that the flow is dominated by gas phase at sensor electrode 3. The voltage reading at bottom sensor electrode is initially lower than the voltage reading at sensor electrode 2 when the gas superficial velocity is low. However, as the gas superficial velocity is increased, the voltage reading at the bottom sensor electrode also started to increase and had less voltage difference as it flows upwards the channel. This proves that gas bubbles began to coalesce quickly as the gas superficial velocity is increased. Meanwhile, from figure 4.3, the lowest voltage reading is at sensor electrode 3, where the channel is dominated by the liquid phase. However, as it moves upward along the channel, the voltage reading started to increase. Hence, it is assumed that the gas bubbles coalesce, resulting in bigger and longer bubbles as it approaches the top of the vertical channel.

4.2.1 Void Fraction and Slip Ratio

Using equation 6 and 7 from earlier section 3.2, the void fraction at each sensor electrodes and slip ratio for each run were calculated. Table 4.3 exhibits the calculated slip ratio and void fraction for each test at every sensor electrodes.

Table 4.3: Experimental Slip Ratio and Void Fraction Results

Liquid Superficial Velocity, j_L	Gas Superficial Velocity, j_G	Slip Ratio, S	Void Fraction 1, α_1 L/D = 20	Void Fraction 2, α_2 L/D = 35	Void Fraction 3, α_3 L/D = 50	Void Fraction 4, α_4 L/D = 65	Void Fraction 5, α_5 L/D = 80
[m/s]	[m/s]	[-]					
	0.0265	0.3732	0.9300	0.8008	0.8517	0.9284	0.9982
	0.0398	0.5606	0.8654	0.7113	0.8313	0.9725	0.9702
	0.0663	0.9338	0.9313	0.8101	0.8550	0.9507	0.9986
	0.0995	1.4014	0.9349	0.8161	0.8577	0.9639	0.9989
	0.1326	1.8676	0.9454	0.8226	0.8587	0.9653	0.9991
0.071	0.1658	2.3352	0.9670	0.8394	0.8607	0.9690	0.9994
	0.1989	2.8014	0.9651	0.8348	0.8602	0.9673	0.9994
	0.2321	3.2690	0.9677	0.8422	0.8660	0.9661	0.9994
	0.2653	3.7366	0.9658	0.8339	0.8612	0.9690	0.9994
	0.3316	4.6704	0.9701	0.8441	0.8665	0.9727	0.9994
	0.3979	5.6042	0.9722	0.8601	0.8597	0.9739	0.9995
	0.0265	0.1167	0.9503	0.7293	0.9753	0.9687	0.8954
	0.0398	0.1753	0.9560	0.7438	0.9759	0.9745	0.9169
	0.0663	0.2921	0.9669	0.7707	0.9751	0.9739	0.9307
	0.0995	0.4383	0.9719	0.8025	0.9772	0.9766	0.9399
	0.1326	0.5841	0.9752	0.8149	0.9761	0.9789	0.9456
0.227	0.1658	0.7304	0.9793	0.8234	0.9783	0.9801	0.9480
	0.1989	0.8762	0.9797	0.8341	0.9768	0.9828	0.9503
	0.2321	1.0225	0.9812	0.8448	0.9864	0.9845	0.9265
	0.2653	1.1687	0.9819	0.8473	0.9859	0.9838	0.9280
	0.3316	1.4608	0.9824	0.8621	0.9863	0.9861	0.9341
	0.3979	1.7529	0.9826	0.8431	0.9797	0.9831	0.9552
	0.0265	0.0668	0.8238	0.9575	0.9054	0.9115	0.8581
	0.0398	0.1003	0.8225	0.9271	0.9153	0.8944	0.8442
	0.0663	0.1670	0.8202	0.9621	0.8958	0.9044	0.8595
	0.0995	0.2506	0.8282	0.9668	0.9203	0.9138	0.8644
	0.1326	0.3340	0.8342	0.9652	0.8850	0.9250	0.8823
0.397	0.1658	0.4176	0.8222	0.9695	0.8992	0.9241	0.8579
	0.1989	0.5010	0.8334	0.9652	0.9065	0.9306	0.8754
	0.2321	0.5846	0.8060	0.9684	0.8960	0.9035	0.8617
	0.2653	0.6683	0.8057	0.9677	0.9078	0.9082	0.8331
	0.3316	0.8353	0.7989	0.9641	0.9354	0.9254	0.8364
	0.3979	1.0023	0.8022	0.9606	0.9400	0.9233	0.8522

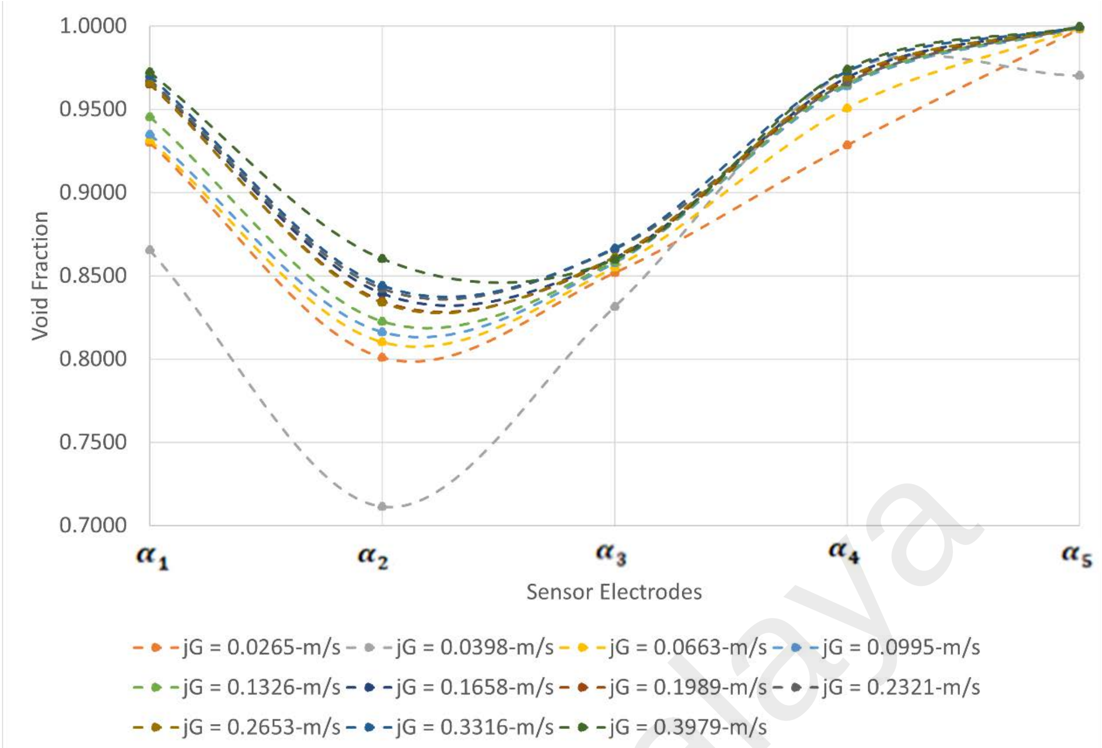

Figure 4.4: Void Fraction at Each Sensor Electrodes With Constant Superficial Velocity, j_L = 0.071-m/s.

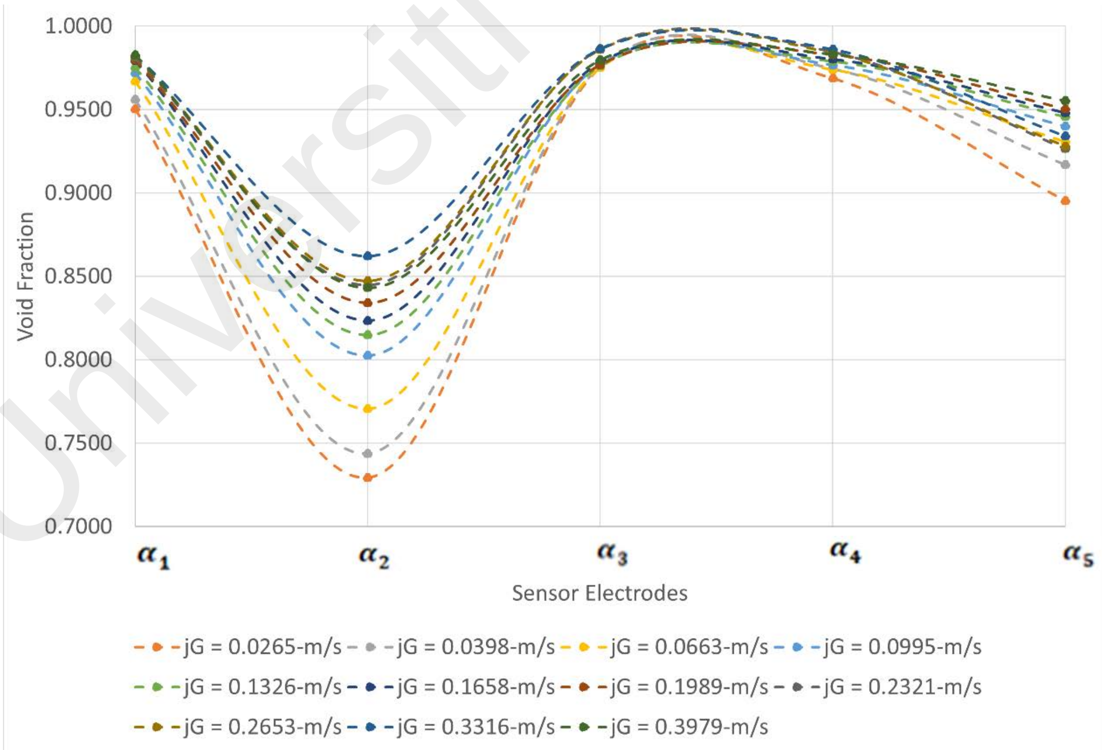

Figure 4.5: Void Fraction at Each Sensor Electrodes With Constant Superficial Velocity, j_L = 0.227-m/s.

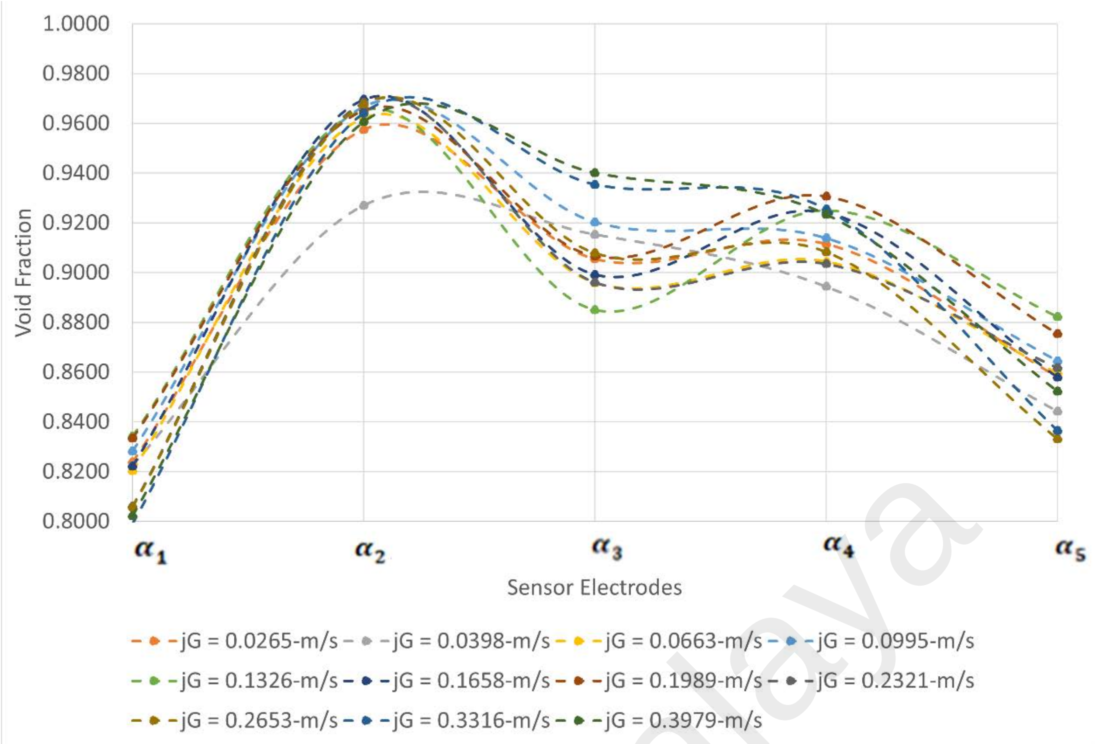

Figure 4.6: Void Fraction at Each Sensor Electrodes With Constant Superficial Velocity, j_L = 0.397-m/s.

Based on Table 4.3, a graphical representation of the void fraction measurement for each fixed liquid superficial velocity, j_L, at 0.071-m/s, 0.227 m/s-and 0.397-m/s are shown in Figure 4.4, 4.5 and 4.6 respectively. For j_L= 0.071-m/s, the highest void fraction value is at the top section, with axial location *L/D* = 80, while the lowest void fraction value is location *L/D* = 35. As gas bubbles are injected into the liquid flow, the channel is dominated by the gas phase but soon disperses as it reaches axial location between *L/D* = 35 to *L/D* = 50 of which the readings were recorded by sensor electrode 2. However, the gas bubbles began to coalesce and created a slug flow which passes through sensor electrode 3. As the flow approaches the top, the 'slug' increases in size along the vertical tube. At higher liquid superficial velocity, j_L= 0.227-m/s, the void fraction graph shows the same trend as the void fraction graph of j_L= 0.071-m/s. The difference between the two graphs is that as the gas superficial velocity increases, which also increases the slip ratio, at j_L= 0.227-m/s, the void fraction at axial location *L/D* = 35 also increases. As the 'slugs' are mostly formed at axial location *L/D* = 35, with higher slip ratio, the void fraction will also increase. This result shows similar trend to experimental research done by Sekoguchi et al. (1989) and Hughmark (1962).

The void fraction result for j_L = 0.397-m/s shows a different trend in comparison to the first two experiments. The void fraction lowest value is at axial location *L/D* = 20, where gas was injected, and peaks at axial location *L/D* = 35. Then, the void fraction value starts to decrease along the upward vertical channel. This implies that the flow was dominated by the liquid phase at axial location *L/D* = 20 passing through sensor electrode 1, while gas phase began to dominate the channel at axial location *L/D* = 35 passing through sensor electrode 2. As the flow reaches the top of the vertical channel, the void fraction value starts to decrease which indicates the 'slugs' had collapsed. This could be due to gravitational force and shear forces from the liquid flow acting on the gas bubbles. This behavior is observed when liquid superficial velocity is higher which causes the slip ratio values to be smaller than the previous two experiments. As the slip ratio values diminishes, the bubbles are swept away along with the liquid along the channel which decreases the void fraction.

4.3 Flow Pattern

Based on the different flow condition, the flow patterns were observed via visual observations. The images of the bubbles were captured through a high-speed video camera with 1080p at 240 fps and 1080p at 30 fps. Flow patterns were captured at each acrylic tubes after the sensor electrodes throughout the experiment. The five sections are at *L/D* = 20 to 35, 25 to 50, 50 to 65, 65 to 80 and 80 to 101 which are Location 1, Location 2, Location 3, Location 4 and Location 5 respectively.

4.3.1 Flow Pattern at j_L = 0.071-m/s

The flow patterns with liquid superficial velocity of 0.071-m/s and varying gas superficial velocity are recorded in Table 4.4. From the table, Location 2, which is the tube between axial location *L/D* = 25 to 50, shows that the flow is dominated by liquid phase in comparison to other sections of the channel. It is also observed that the bubbles became bigger and longer as it approached the top of the channel. Similarly, as the gas superficial velocity is increased, bigger and longer slugs are seen. The flow pattern types for the experimental run with liquid superficial velocity of 0.071-m/s are only bubbly flow and slug flow. Even at a higher gas superficial velocity, the slugs formed did not reach an unstable state which could break off into different shapes. Instead, the slugs maintained its spherical head as it flows upward along the channel.

Table 4.4: Flow Pattern at j_L = 0.071-m/s

Gas Superficial Velocity, j_G [m/s]	Location 1 L/D = 20 to 35	Location 2 L/D = 35 to 50	Location 3 L/D = 50 to 65	Location 4 L/D = 65 to 80	Location 5 L/D = 80 to 101
0.0265	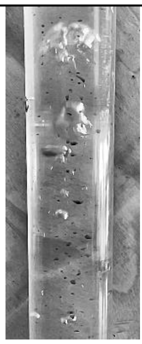		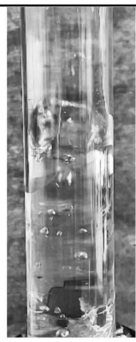		
0.0398			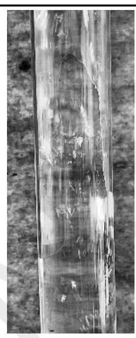		
0.0663			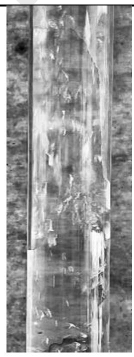		
0.0995			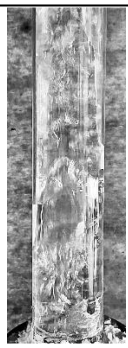		

0.1326			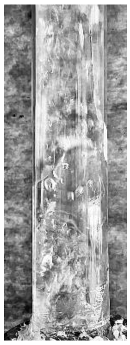		
0.1658	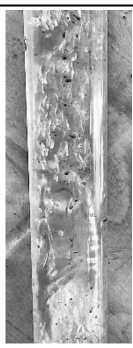			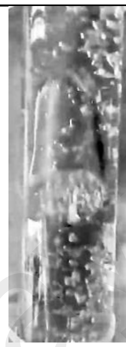	
0.1989	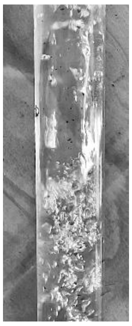				
0.2321					
0.2653					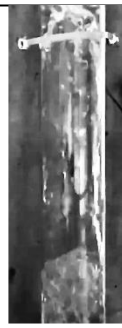

0.3316	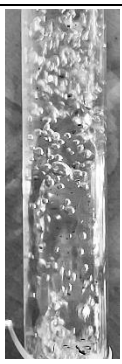				
0.3979			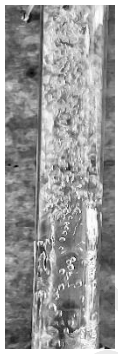		

4.3.2 Flow Pattern at j_L = 0.227 m/s

Referring to Table 4.5, the flow pattern when liquid superficial velocity is 0.227-m/s is similar to when liquid superficial velocity is 0.071-m/s. The slugs get bigger and longer with increasing gas superficial velocity and as it flows upward the vertical channel. Location 2 which is the tube at axial location *L/D* = 35 to 50 is dominated by the liquid phase in comparison to other locations. The difference between the two flow is that flow pattern at axial location *L/D* = 65 to 80, which is after sensor electrode 4, showed that the flow is dominated by gas phase. This is due to higher gas superficial velocity which caused the slugs to become unstable as it reaches the top of the channel. Hence, the slugs broke off and the void between the separated bubbles caused the liquid to backflow downwards due to the effect of gravitational force on the liquid film. Therefore, at liquid superficial velocity of 0.227-m/s, bubbly flow, slug flow and churn flow existed.

Table 4.5: Flow Pattern at j_L = 0.227-m/s

Gas Superficial Velocity, j_G [m/s]	Location 1 L/D = 20 to 35	Location 2 L/D = 35 to 50	Location 3 L/D = 50 to 65	Location 4 L/D = 65 to 80	Location 5 L/D = 80 to 101
0.0265	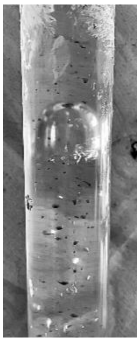				
0.0398		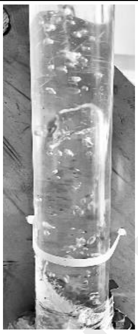			
0.0663					
0.0995					

0.1326	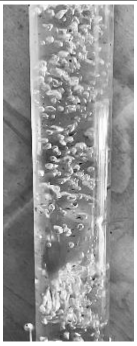		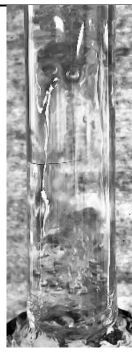		
0.1658					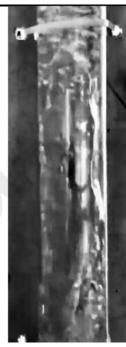
0.1989			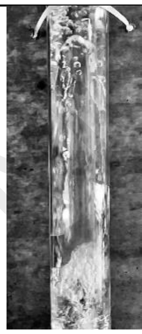		
0.2321					
0.2653			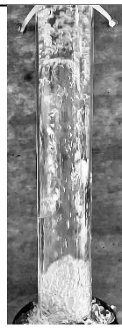		

0.3316		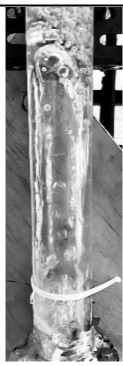	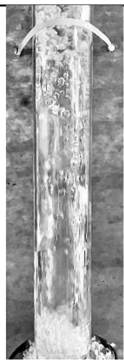		
0.3979			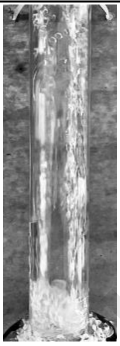		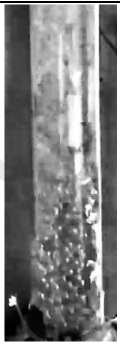

4.3.3 Flow Pattern at j_L = 0.397 m/s

Based on Table 4.6, at liquid superficial velocity of 0.397-m/s, bigger slugs are formed quickly in comparison to the previous two experimental run. However, slugs at axial location *L/D* = 35 to 50, which is after sensor electrode 2, showed bigger slugs in comparison to slugs at axial location *L/D* = 20 to 35. With increasing gas superficial velocity, bigger slugs at axial location *L/D* = 35 to 50 became unstable and broke off, allowing liquid backflow, thus dominated by liquid phase at axial location *L/D* = 50 to 65. As gas superficial velocity increased, the higher interfacial shear forces caused the slugs to travel upward. Slugs that collapsed from the top of the channel caused liquid backflow due to gravitational force on the liquid film, where churn flow was observed. For liquid superficial velocity of 0.397-m/s, bubbly flow, slug flow and churn flow were observed.

Table 4.6: Flow Pattern at j_L = 0.397 m/s

Gas Superficial Velocity, j_G [m/s]	Location 1 L/D = 20 to 35	Location 2 L/D = 35 to 50	Location 3 L/D = 50 to 65	Location 4 L/D = 65 to 80	Location 5 L/D = 80 to 101
0.0265					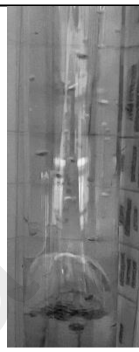
0.0398					
0.0663			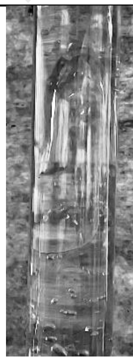		
0.0995					

0.1326					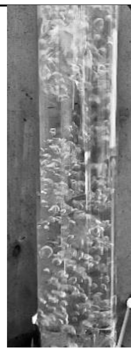
0.1658					
0.1989		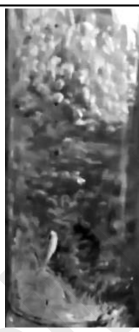			
0.2321		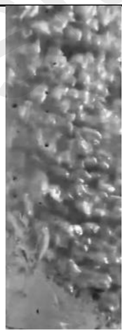			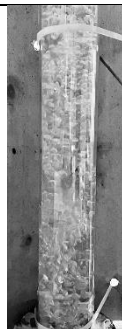
0.2653	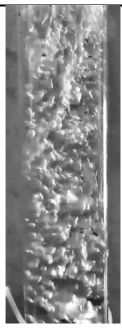	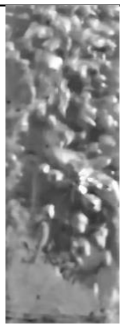	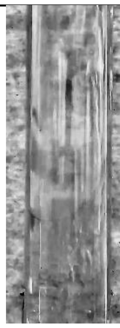	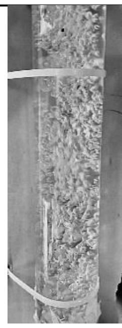	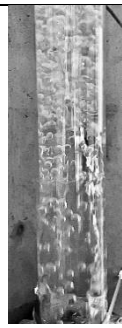

0.3316		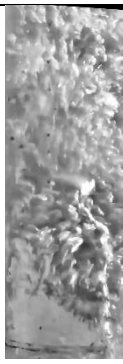	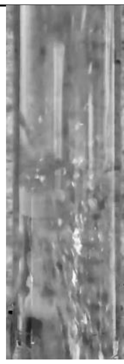		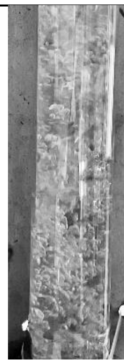
0.3979				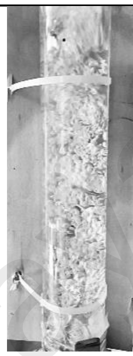	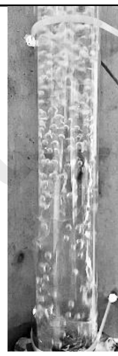

4.4 Actual Bubble Velocity

As per section 3.4, the velocity of the gas bubbles can be calculated based on the voltage fluctuation generated from LabVIEW® during the experimental run. The voltage fluctuations of each run are included in the Appendices, Figure 0.1 ~ 0.35, of this report. In this work, void fraction profiles at different axial location are used to calculate the actual bubble velocity. For this purpose, these profiles were plotted on the same diagram, with spectral fluctuation against time. As shown in Figure 4.7, similar profiles of different spectral show the time-lapse flow of the same bubble or its trails at different channel locations with a known length, L_x. Therefore, the actual bubble velocity can be calculated using Equation 8 from section 3.2.3.

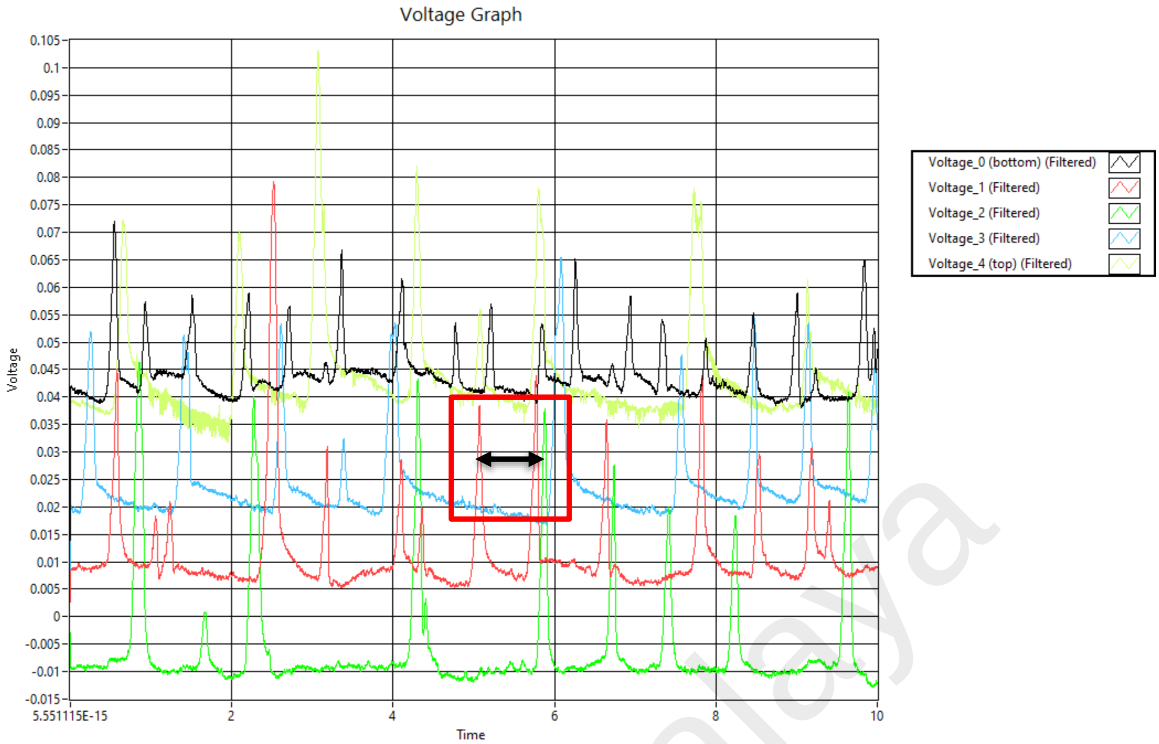

Figure 4.7: LabVIEW Voltage Spectrum for Each Sensor Electrodes at j_L = 0.397-m/s and j_G = 0.0398-m/s (3-L/min).

The calculated actual bubble velocities are tabulated in Table 4.7 while graphically represented through Figure 4.8, 4.9 and 4.10 for liquid superficial velocity, j_L, of 0.071-m/s, 0.227-m/s and 0.397-m/s respectively. Based on Figure 4.8 ~ 4.10, the actual bubble velocities are in an upward trend as the it reaches the top of the vertical channel. With increasing gas superficial velocities, the bubble velocity also increased. The difference between the three tests is that for experimental run with lower gas superficial velocity, the actual bubble velocities, v_b, are higher when liquid superficial velocity, j_L = 0.071-m/s. However, as the gas superficial velocities, j_G, increased, the actual bubble velocity at liquid superficial velocity, j_L = 0.071-m/s, is lower compared to the higher liquid superficial velocities of 0.227-m/s and 0.397-m/s. This can be inferred as the actual bubble velocity to increase with both higher liquid superficial velocities and higher gas superficial velocities.

Table 4.7: Actual Bubble Velocity Experimental Results

Liquid Superficial Velocity, j_L	Gas Superficial Velocity, j_G	Slip Ratio, S	Actual Bubble Velocity, v_b			
			L/D = 20 to 35	*L/D* = 35 to 50	*L/D* = 50 to 65	*L/D* = 65 to 80
[m/s]	[m/s]	[-]	[m/s]			
0.071	0.0265	0.3732	0.3203	0.3486	0.3521	0.3692
	0.0398	0.5606	0.3727	0.3793	0.3836	0.3924
	0.0663	0.9338	0.3822	0.3937	0.4167	0.4222
	0.0995	1.4014	0.3819	0.4043	0.4286	0.4313
	0.1326	1.8676	0.3945	0.4104	0.4360	0.4332
	0.1658	2.3352	0.4342	0.4633	0.4878	0.5357
	0.1989	2.8014	0.4619	0.5797	0.5263	0.7344
	0.2321	3.2690	0.5450	0.5758	0.6734	0.7519
	0.2653	3.7366	0.6309	0.6501	0.7772	0.8368
	0.3316	4.6704	0.7792	0.7853	0.8119	0.8696
	0.3979	5.6042	0.8197	0.8596	0.9317	1.1364
0.227	0.0265	0.1167	0.2938	0.3155	0.3333	0.3436
	0.0398	0.1753	0.3106	0.3122	0.3299	0.3367
	0.0663	0.2921	0.3263	0.3482	0.3659	0.3748
	0.0995	0.4383	0.3367	0.3750	0.3797	0.4164
	0.1326	0.5841	0.3612	0.4104	0.4380	0.5008
	0.1658	0.7304	0.3924	0.4532	0.4886	0.5550
	0.1989	0.8762	0.4161	0.4992	0.4992	0.6000
	0.2321	1.0225	0.4573	0.5455	0.5820	0.6795
	0.2653	1.1687	0.5115	0.5505	0.6237	0.7264
	0.3316	1.4608	0.5650	0.5820	0.6952	0.7326
	0.3979	1.7529	0.5929	0.7585	0.8357	0.8772
0.397	0.0265	0.0668	0.2749	0.2761	0.3020	0.3072
	0.0398	0.1003	0.3030	0.3542	0.3672	0.3919
	0.0663	0.1670	0.3608	0.3805	0.3856	0.3886
	0.0995	0.2506	0.4040	0.4481	0.4619	0.6593
	0.1326	0.3340	0.4751	0.5376	0.5213	0.5666
	0.1658	0.4176	0.5333	0.5396	0.5479	0.6667
	0.1989	0.5010	0.5435	0.5520	0.6682	0.6952
	0.2321	0.5846	0.5894	0.6336	0.6615	0.6985
	0.2653	0.6683	0.7212	0.7557	0.7905	0.8403
	0.3316	0.8353	0.7752	0.8511	0.8837	1.0471
	0.3979	1.0023	0.8119	0.9852	1.0435	1.4184

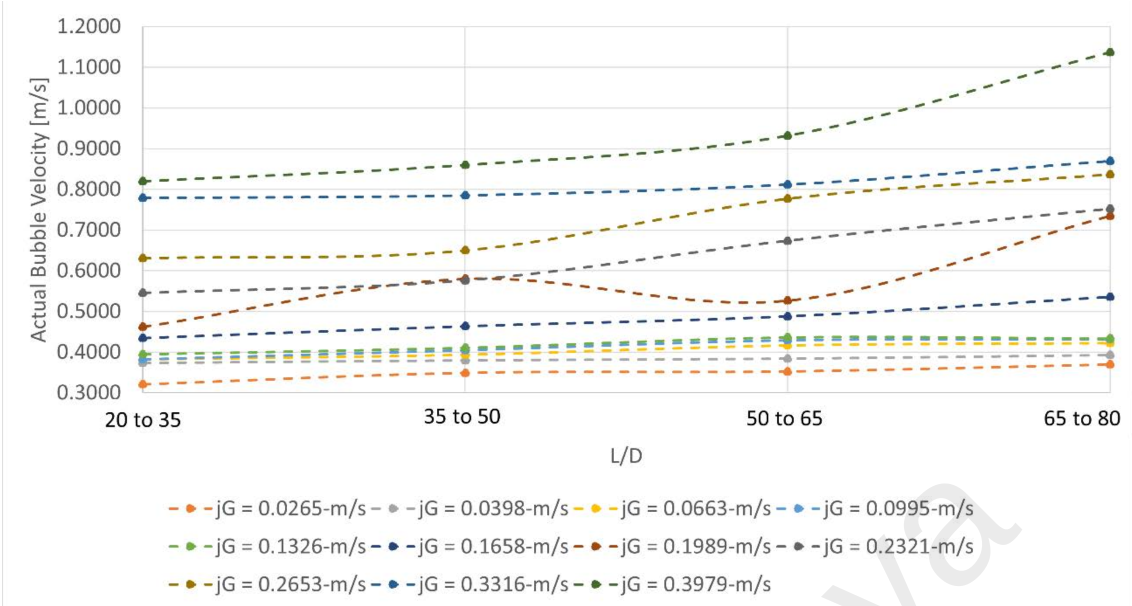

Figure 4.8: Actual Bubble Velocity Along Vertical Tube With Constant Superficial Velocity, j_L = 0.071-m/s.

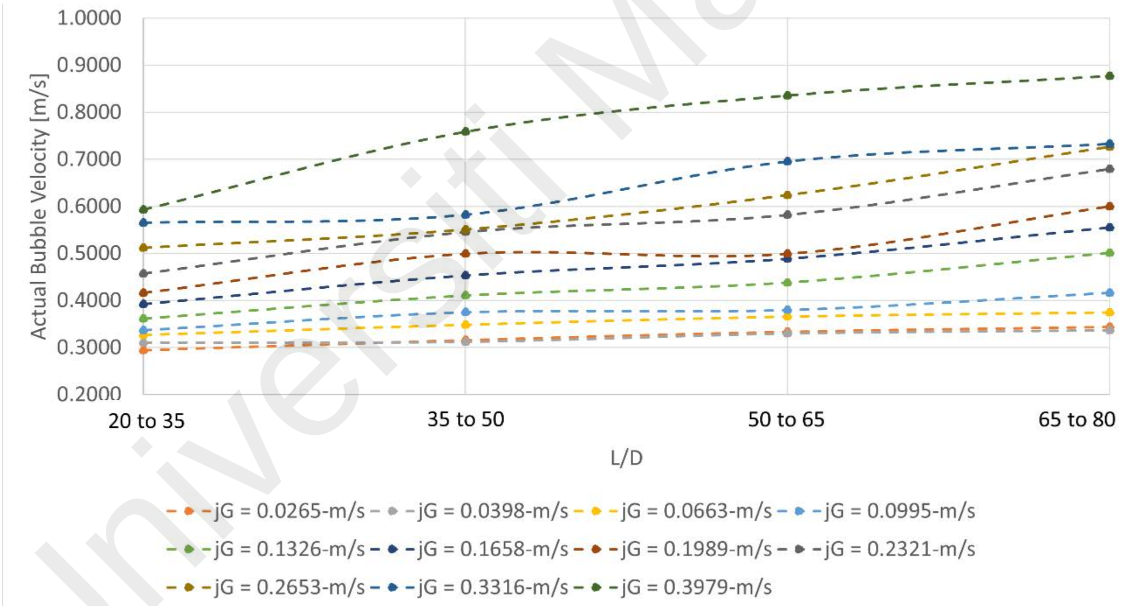

Figure 4.9: Actual Bubble Velocity Along Vertical Tube With Constant Superficial Velocity, j_L = 0.227-m/s.

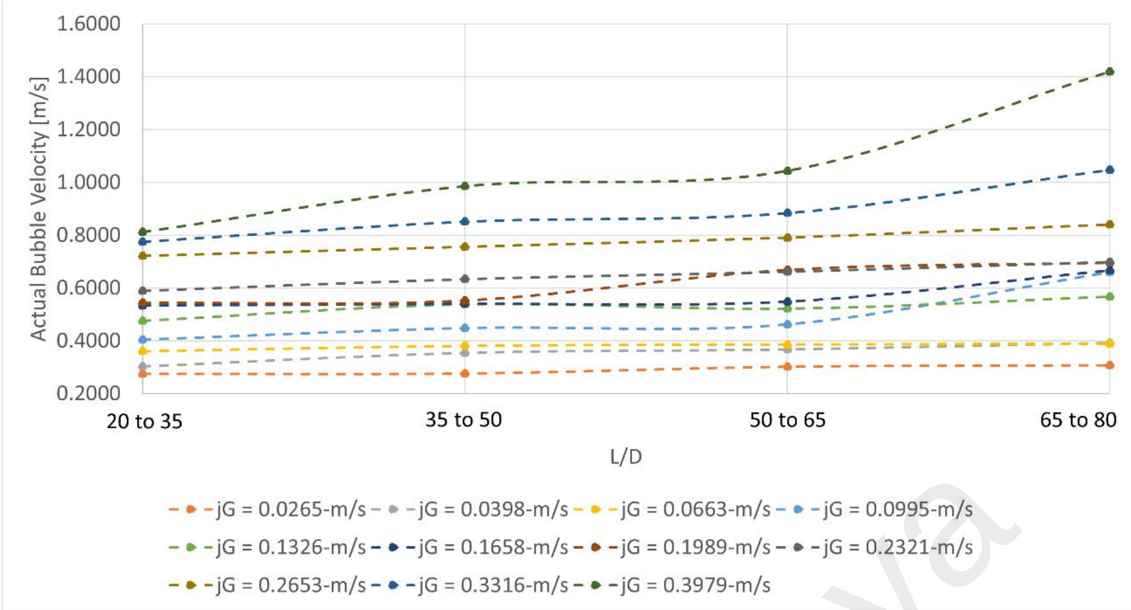

Figure 4.10: Actual Bubble Velocity Along Vertical Tube With Constant Superficial Velocity, j_L = 0.397-m/s.

CHAPTER 5: CONCLUSION AND FUTURE WORK

5.1 Conclusion

In order to prevent the loss of coolant accident (LOCA) such as the Fukushima Disaster in 2011, extensive research were done involving two-phase flow to improve the design of piping systems for efficient cooling system. By utilizing an industrial scale vertical tube of gas-liquid two-phase flow at the Thermal-hydraulics Laboratory at University of Malaya, various parameters were observed when a series of experimentations were conducted by varying gas and liquid flow rates. The voltage fluctuations were obtained for each run at each sensor electrodes using the Constant Electric Current Method (CECM). The method has been proven accurate and reliable by other researchers while also being the simplest method to observe two-phase flow behavior. Voltage fluctuations obtained from the experiment were used to calculate the void fraction and actual bubble velocity for this work. Flow patterns are also verified based on the voltage fluctuations.

The void fraction of air-water two-phase flow in a vertical tube with 40-mm diameter and 3-m height were measured at three different liquid superficial velocity with varying gas superficial velocities. The results obtained were compared to other researchers' studies and showed similar trends albeit the void fraction values differences due to different working conditions and experimental set up. According to the results, void fraction increases as slip ratio increases. In other words, maximum void fraction was yielded with the lowest liquid superficial velocity, j_L = 0.071-m/s and highest gas superficial velocity, j_G = 0.3979-m/s.

At a constant liquid superficial velocity, the results also show that the value of void fraction increases with increasing gas superficial velocities. As gas superficial velocity increases, the mass flow rate in the channel also increases which results in quicker bubble coalescence to create bigger and longer bubbles slugs as it flows upwards the vertical channel. The void fraction results also show that with higher liquid superficial velocity, specifically to the experiment at j_L = 0.397-m/s, the void fraction value decreases as it reaches the top of the flow channel. This is because the bubbles are unable to retain their local positions, hence were swept away by the liquid. To prove the theory, an experiment with higher liquid superficial velocity was run and the flow pattern observed remained as bubble flow although the gas superficial velocity was increased.

Flow patterns are significant to validate the void fraction results obtained. Conforming to findings in Chapter 2 of this paper, with increasing gas flow, the flow patterns developed from bubbly flow into slug flow and slug flow into churn flow. However, with limited gas superficial velocity, annular flow was not observed in any of these experiments. As the flow patterns were captured at different axial positions, *L/D*, along the vertical tube, it is observed that higher *L/D* yielded higher void fraction than lower *L/D* location. As gas bubbles travelled upwards the vertical tube, longer and bigger bubbles were formed which impacts the void fraction.

As the gas flow is only set as superficial velocity, the actual velocity of gas bubble is not accurately known. However, using the voltage fluctuation obtained from running the experiments, actual bubble velocities were calculated for each run. The results revealed that maximum actual bubble velocity is formed at the highest liquid superficial velocity and highest gas superficial velocity. However, as all experiment did not generate an annular flow pattern, the location of dryout could not be determined along the vertical channel.

In conclusion, this study is considered successful as all objectives were achieved. Besides that, the results were compared with other credible sources and showed the expected trend. CECM is proven to be a reliable method to investigate the void fractions, actual bubble velocity and flow patterns in a vertical channel for co-current air-water two-phase flow.

5.2 Future Work

The parameters of two-phase flow such as the void fraction, flow pattern and actual bubble velocity were explored fully using the constant electrical current method in this study. By running three sets of experiments at three fixed liquid superficial velocities with varying gas superficial velocities, the objectives of this study could be improved further based on the following suggestions:

1. As the study should be on two-phase flow focusing on cooling system, the use of steam will yield significant result in the design of a more efficient cooling system. By using steam as the gas flow and distilled water as the liquid flow, temperature sensors or thermocouples should be installed along the vertical channel to observe the effect of temperature on two-phase flow void fractions and flow patterns.
2. The annular flow was not developed due to the current experimental rig capability, perhaps the use of steam and higher gas flow rate for future experiments will yield significant results to investigate the dryout location.
3. The actual velocities of bubbles could be captured more accurately if there are also high-speed cameras set up to record the time taken for the bubble to travel at each intended axial positions.
4. Reliable high-speed cameras should be installed at each axial positions which requires flow patterns observation so that all images of flow patterns could be taken simultaneously at time, *t*.

APPENDICES

Appendix A: LabVIEW® Voltage Fluctuation Output for Each Experiment

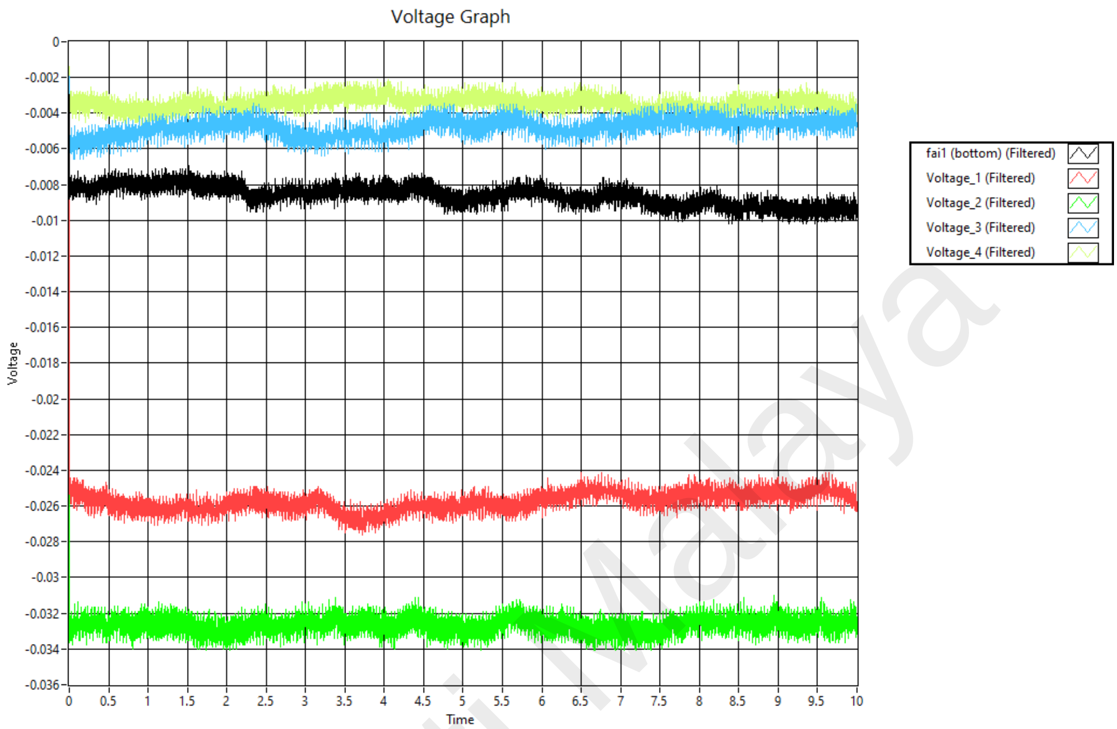

Figure 0.1: Voltage Fluctuation at j_L = 0.071-m/s and j_G = 0-m/s.

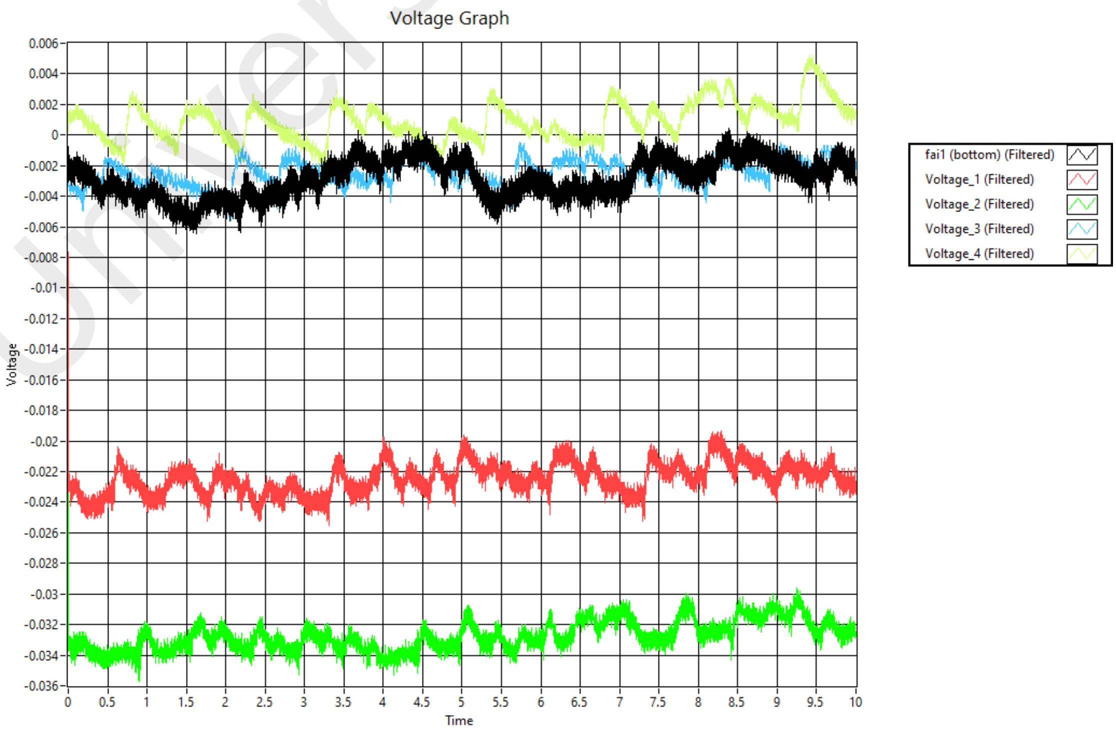

Figure 0.2: Voltage Fluctuation at j_L = 0.071-m/s and j_G = 0.0265-m/s.

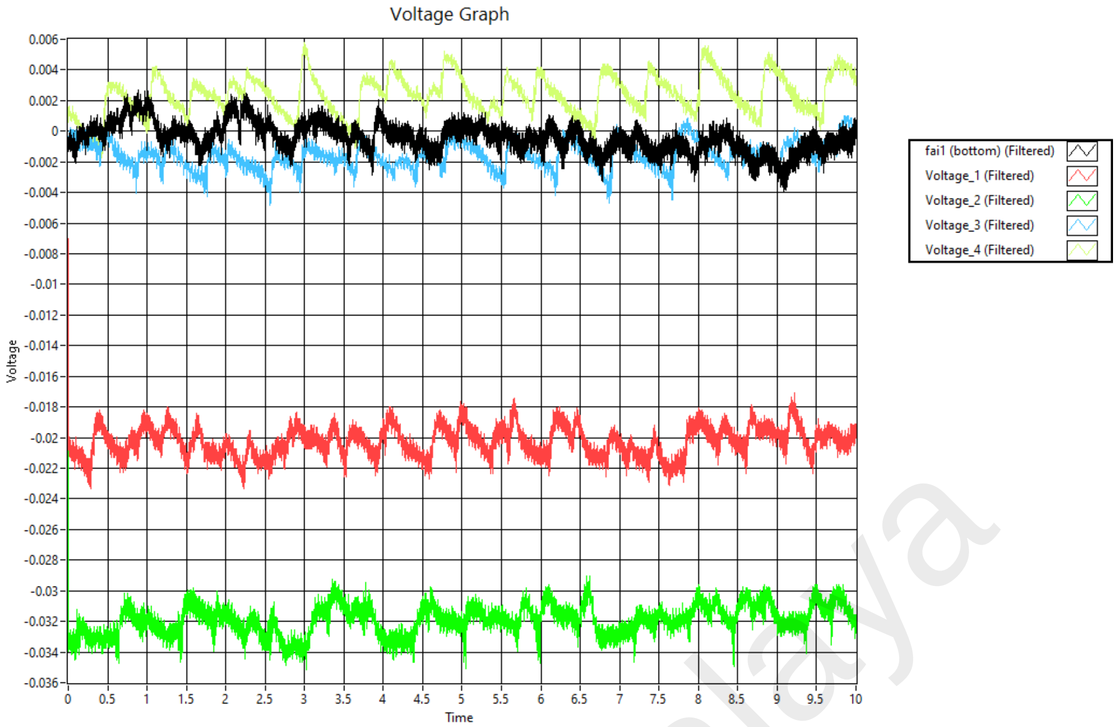

Figure 0.3: Voltage Fluctuation at j_L = 0.071-m/s and j_G = 0.0398-m/s.

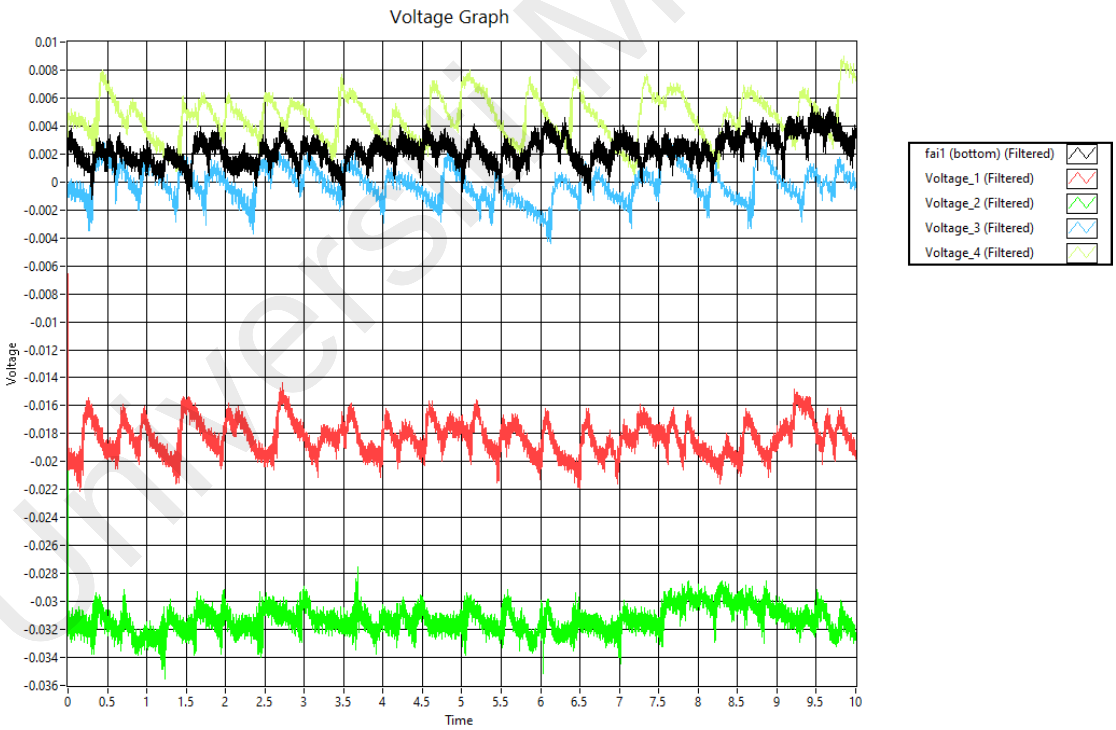

Figure 0.4: Voltage Fluctuation at j_L = 0.071-m/s and j_G = 0.0663-m/s.

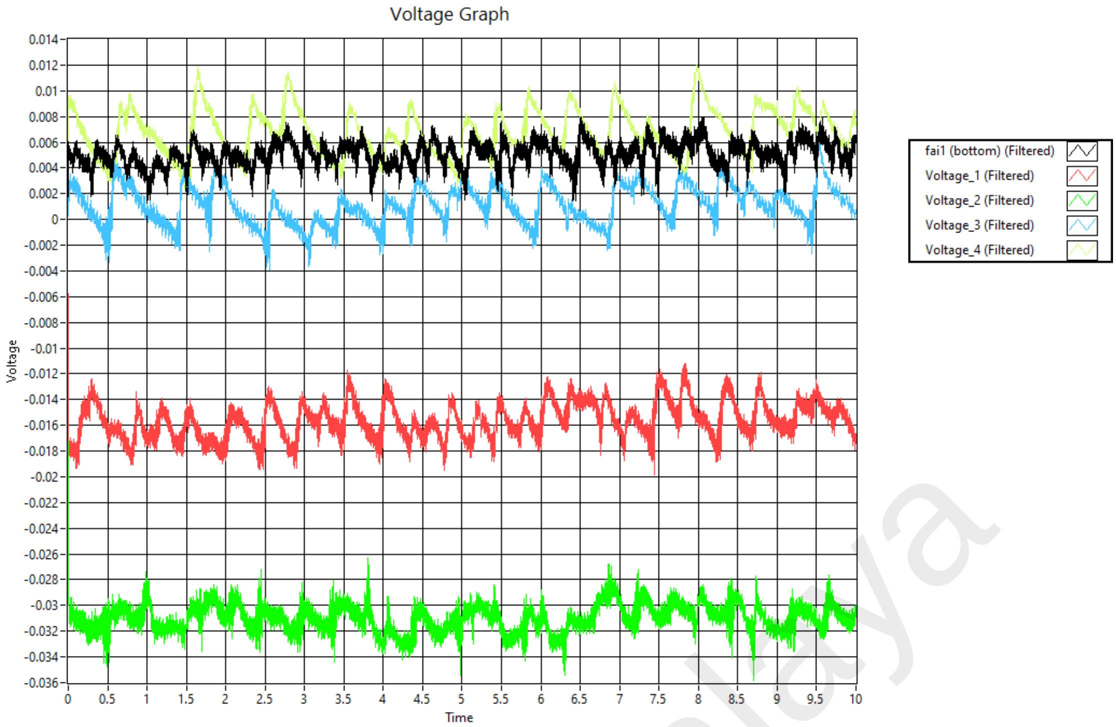

Figure 0.5: Voltage Fluctuation at j_L = 0.071-m/s and j_G = 0.0995-m/s.

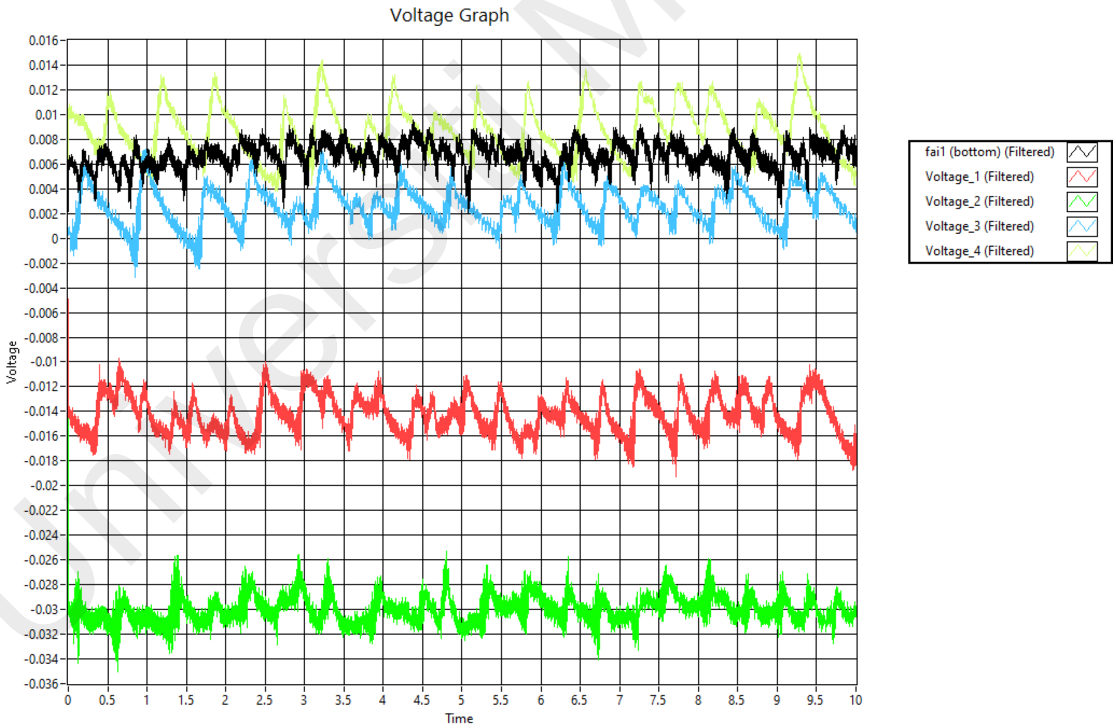

Figure 0.6: Voltage Fluctuation at j_L = 0.071-m/s and j_G = 0.1326-m/s.

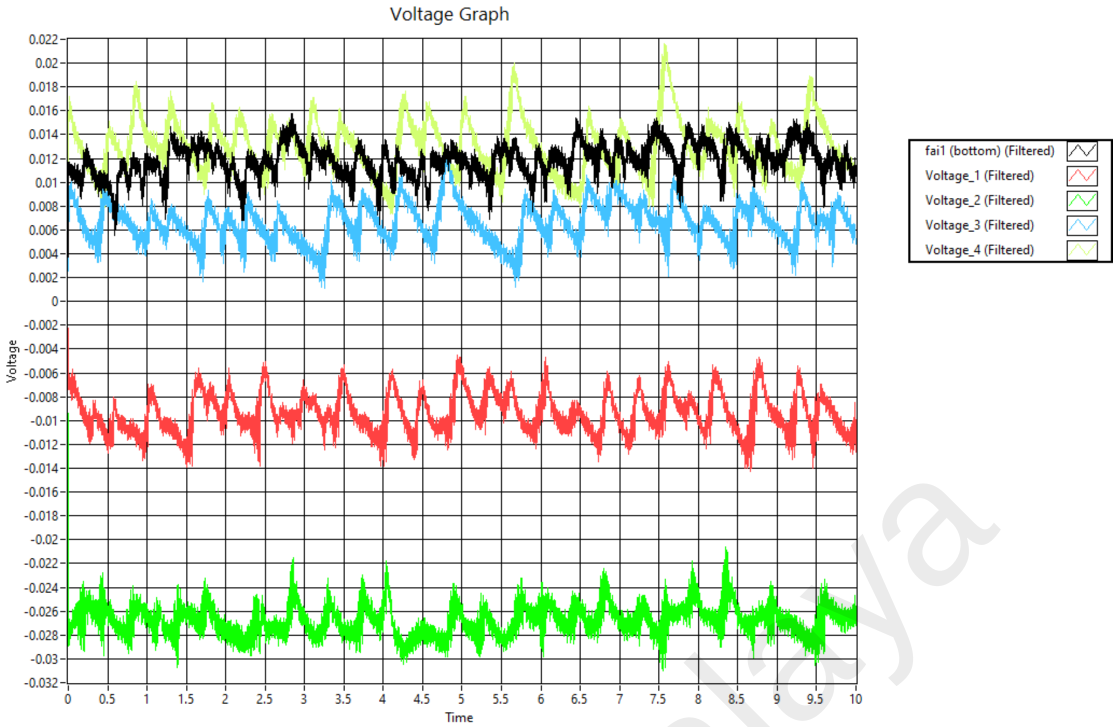

Figure 0.7: Voltage Fluctuation at j_L = 0.071-m/s and j_G = 0.1658-m/s.

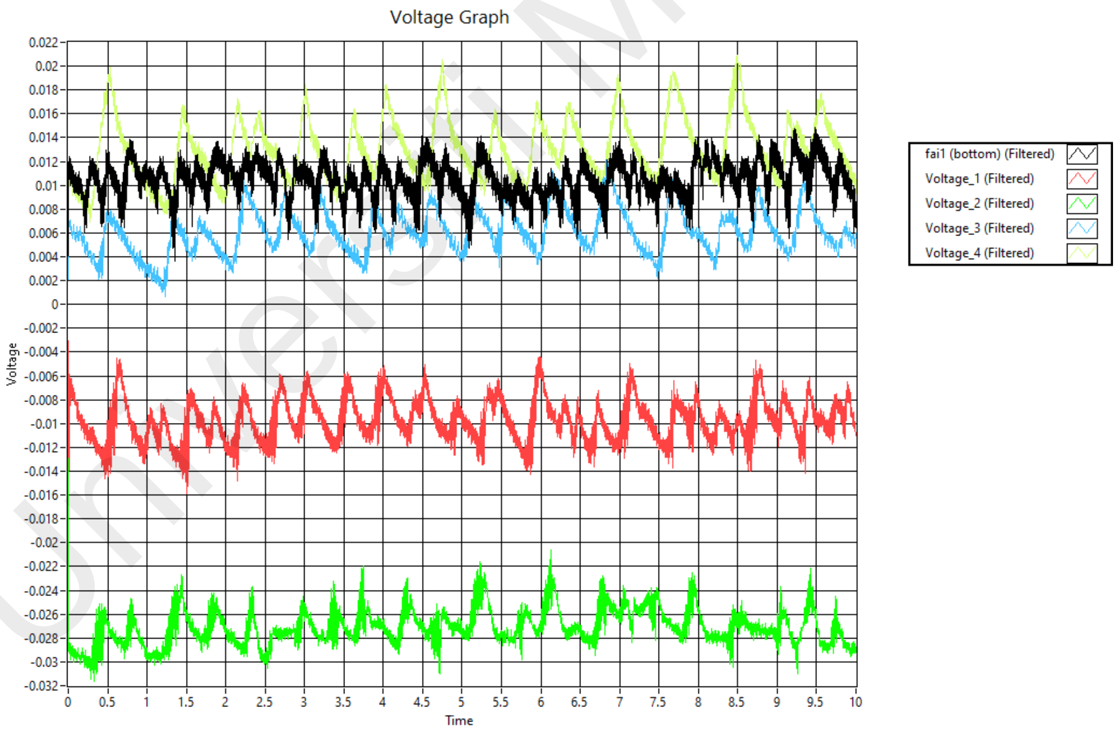

Figure 0.8: Voltage Fluctuation at j_L = 0.071-m/s and j_G = 0.1989 -m/s.

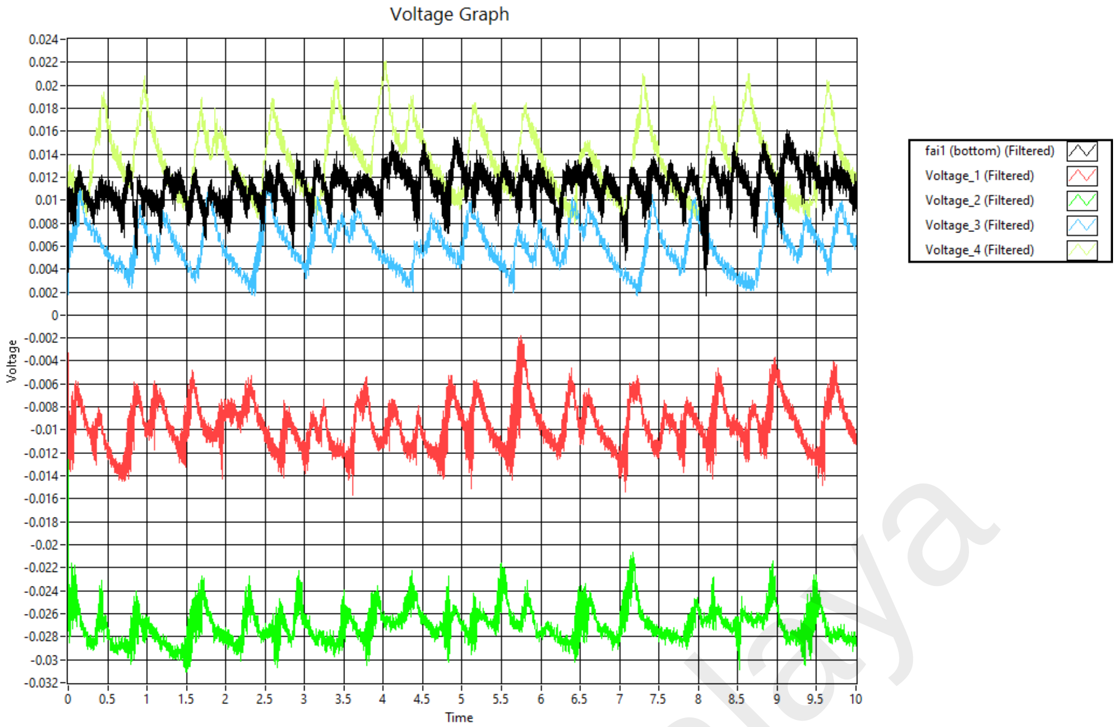

Figure 0.9: Voltage Fluctuation at j_L = 0.071-m/s and j_G = 0.2321-m/s.

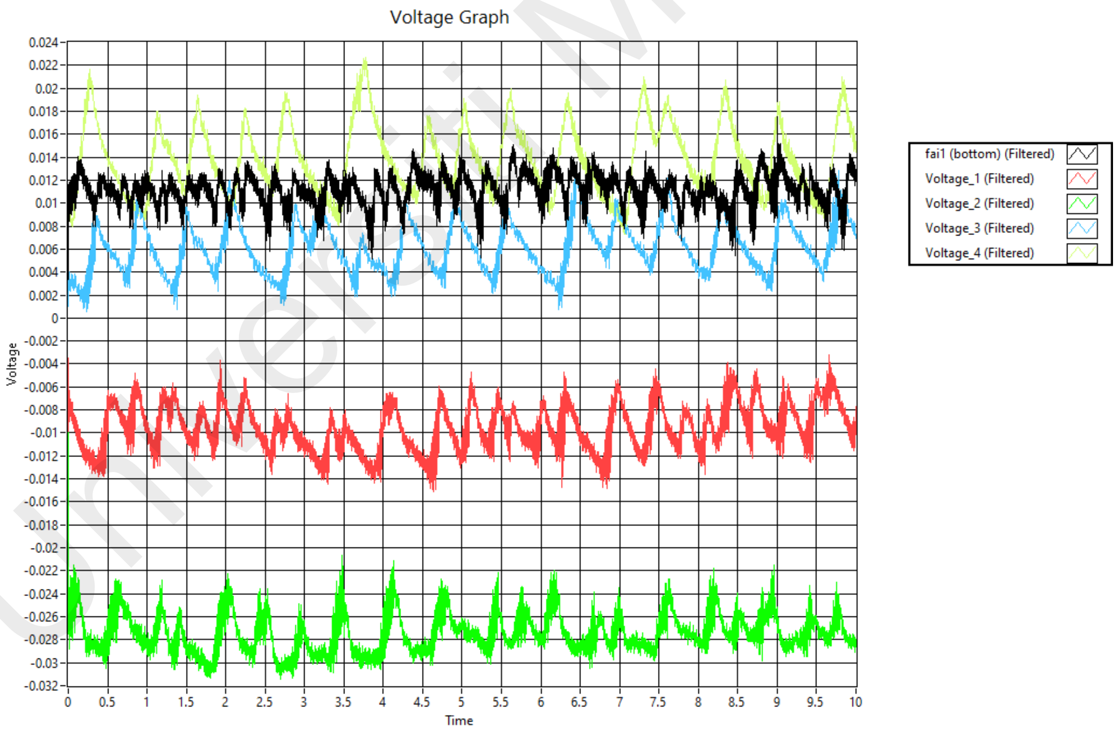

Figure 0.10: Voltage Fluctuation at j_L = 0.071-m/s and j_G = 0.2653-m/s.

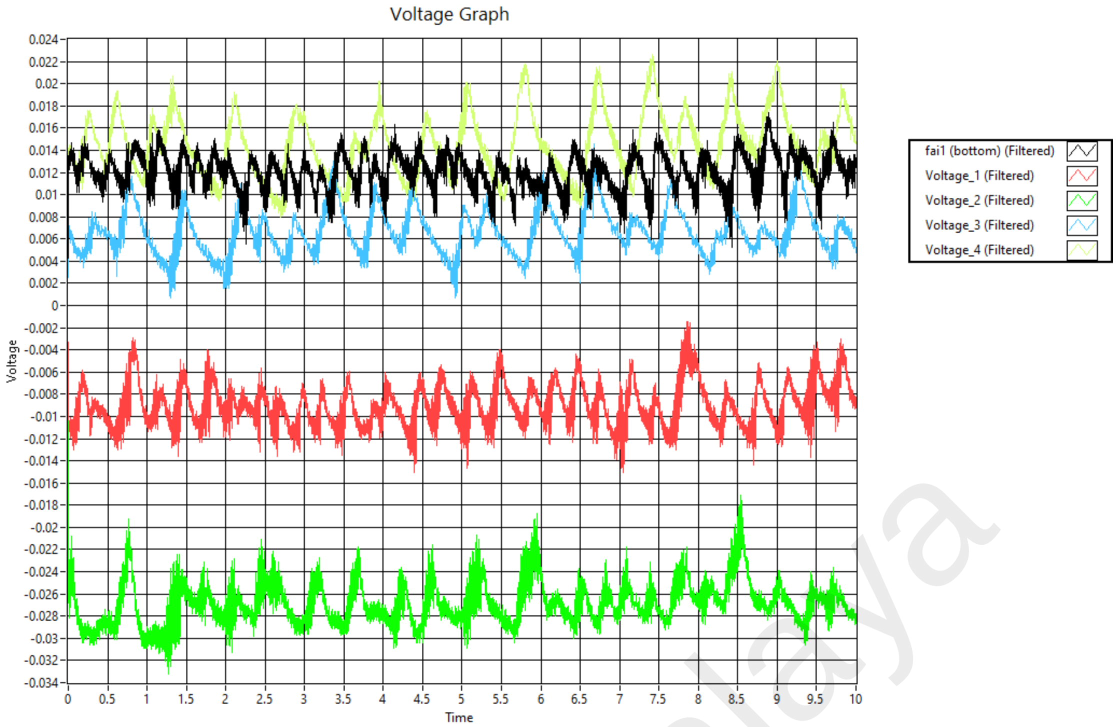

Figure 0.11: Voltage Fluctuation at j_L = 0.071-m/s and j_G = 0.3316 -m/s.

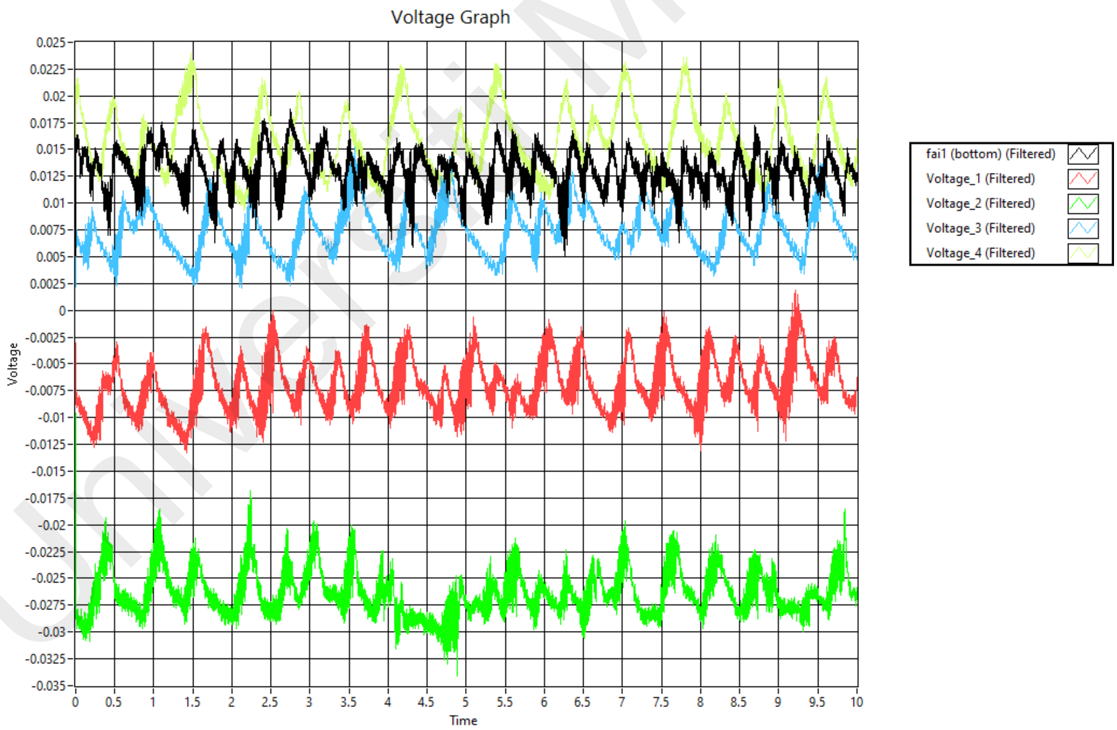

Figure 0.12: Voltage Fluctuation at j_L = 0.071-m/s and j_G = 0.3979-m/s.

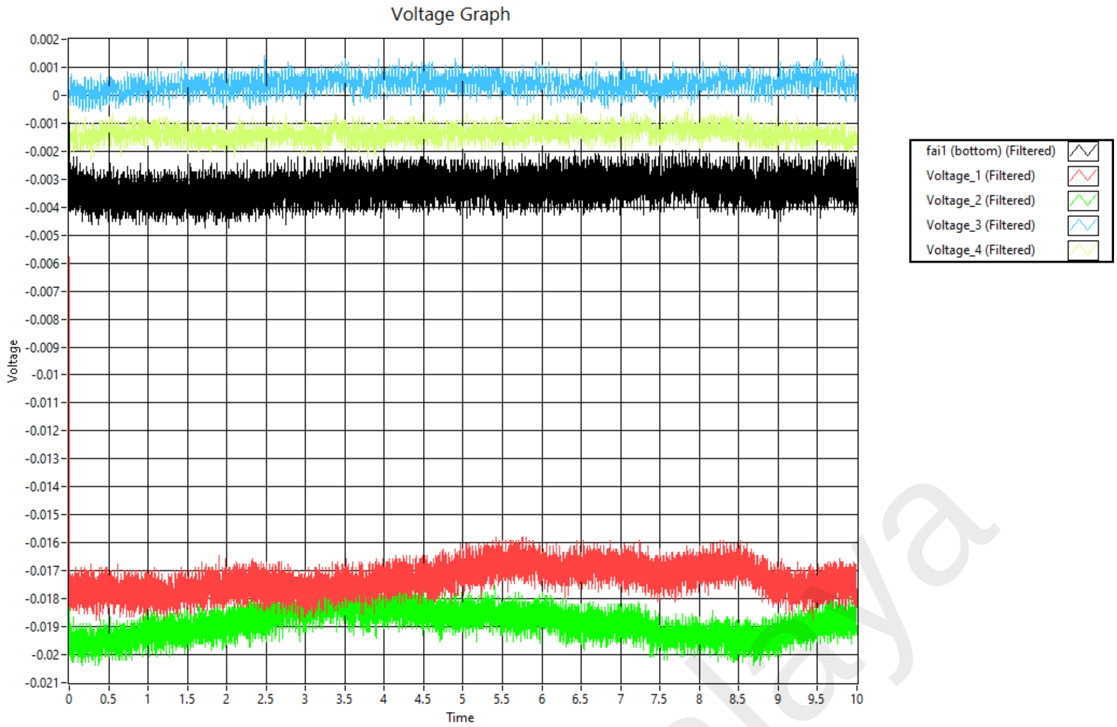

Figure 0.13: Voltage Fluctuation at j_L = 0.227-m/s and j_G = 0-m/s.

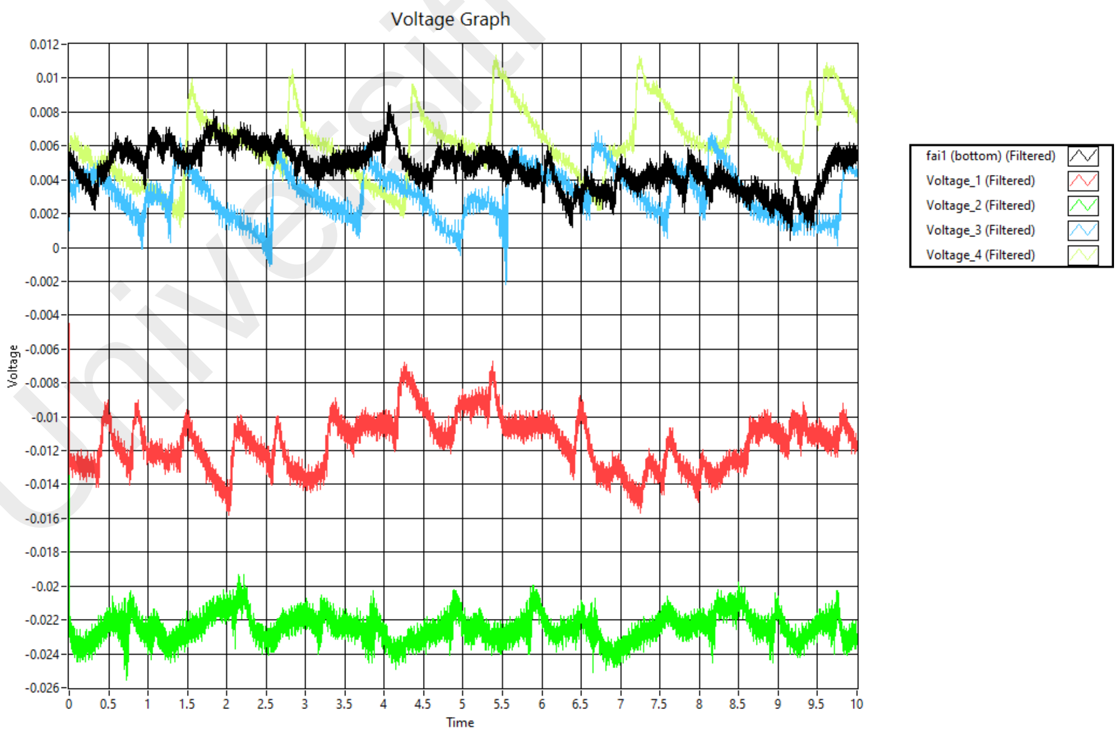

Figure 0.14: Voltage Fluctuation at j_L = 0.227-m/s and j_G = 0.0265-m/s.

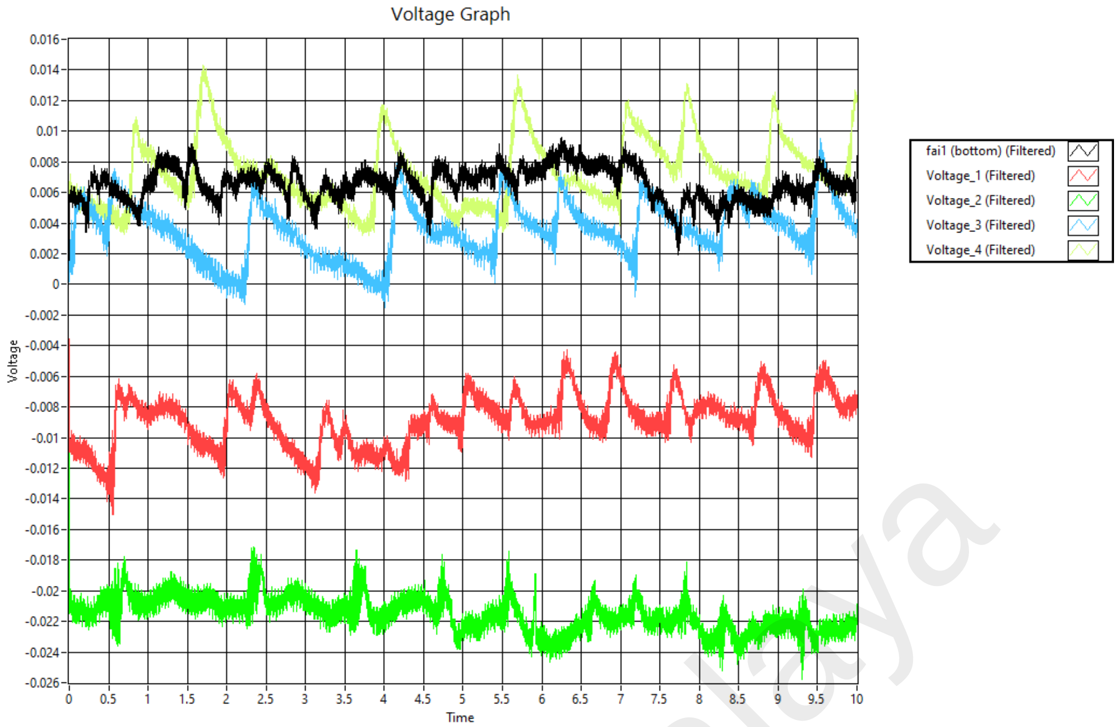

Figure 0.15: Voltage Fluctuation at j_L = 0.227-m/s and j_G = 0.0398-m/s.

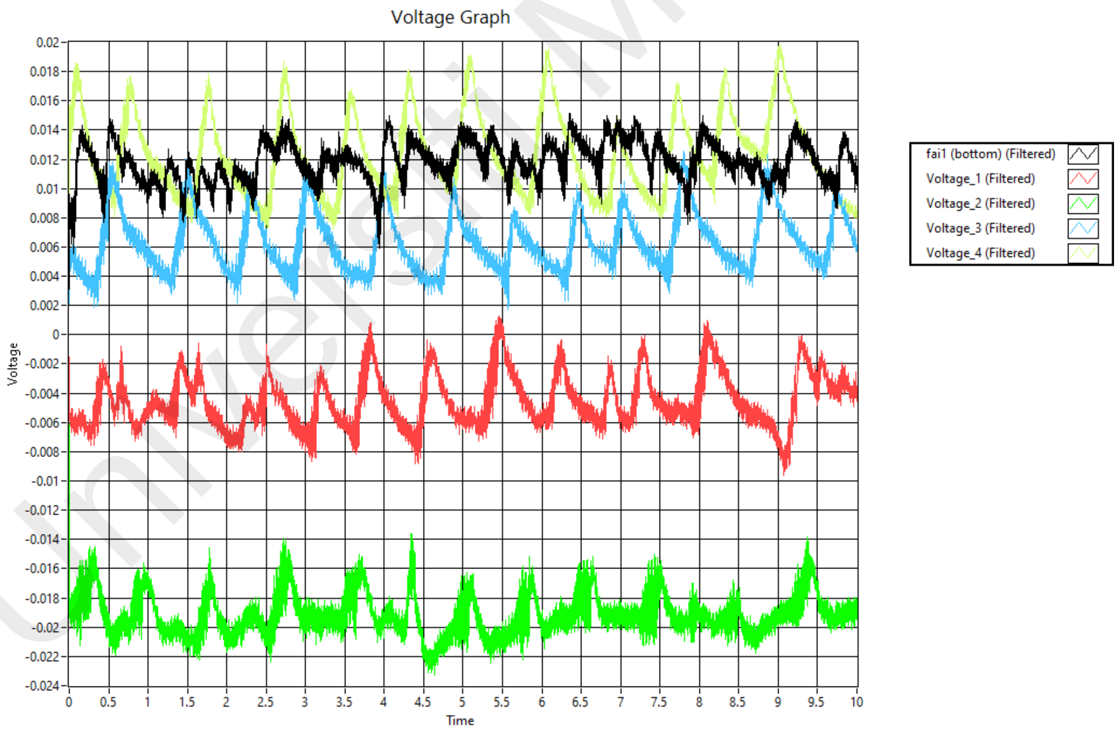

Figure 0.16: Voltage Fluctuation at j_L = 0.227-m/s and j_G = 0.0663-m/s.

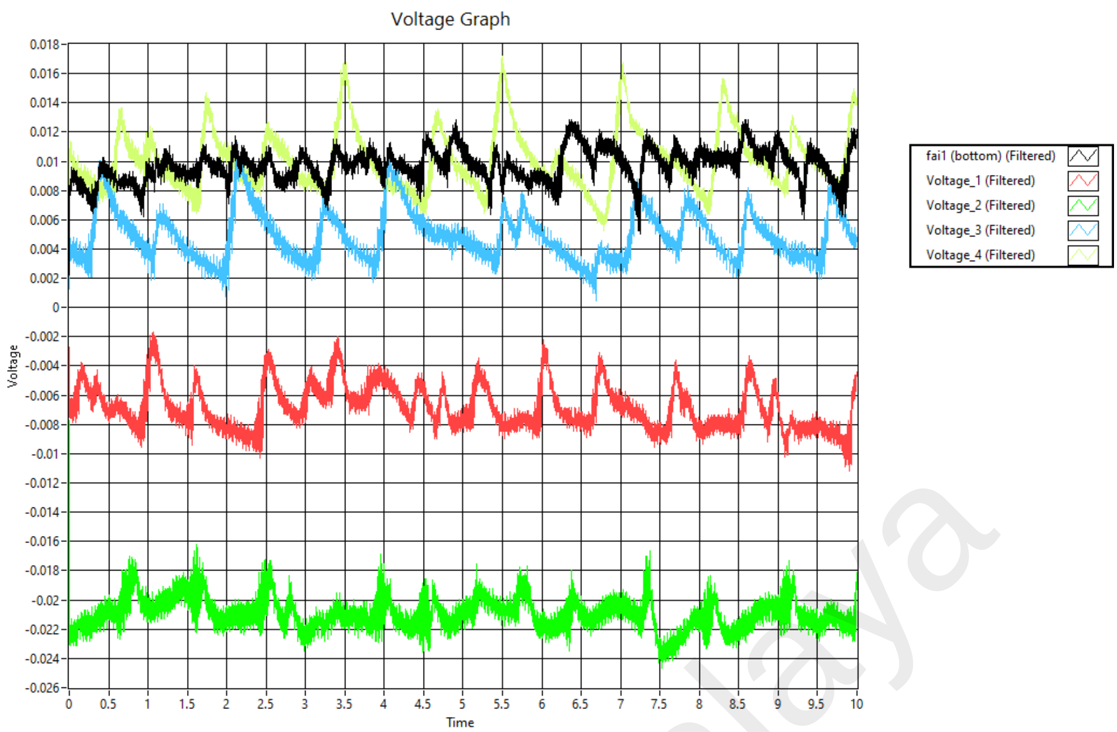

Figure 0.17: Voltage Fluctuation at j_L = 0.227-m/s and j_G = 0.0995-m/s.

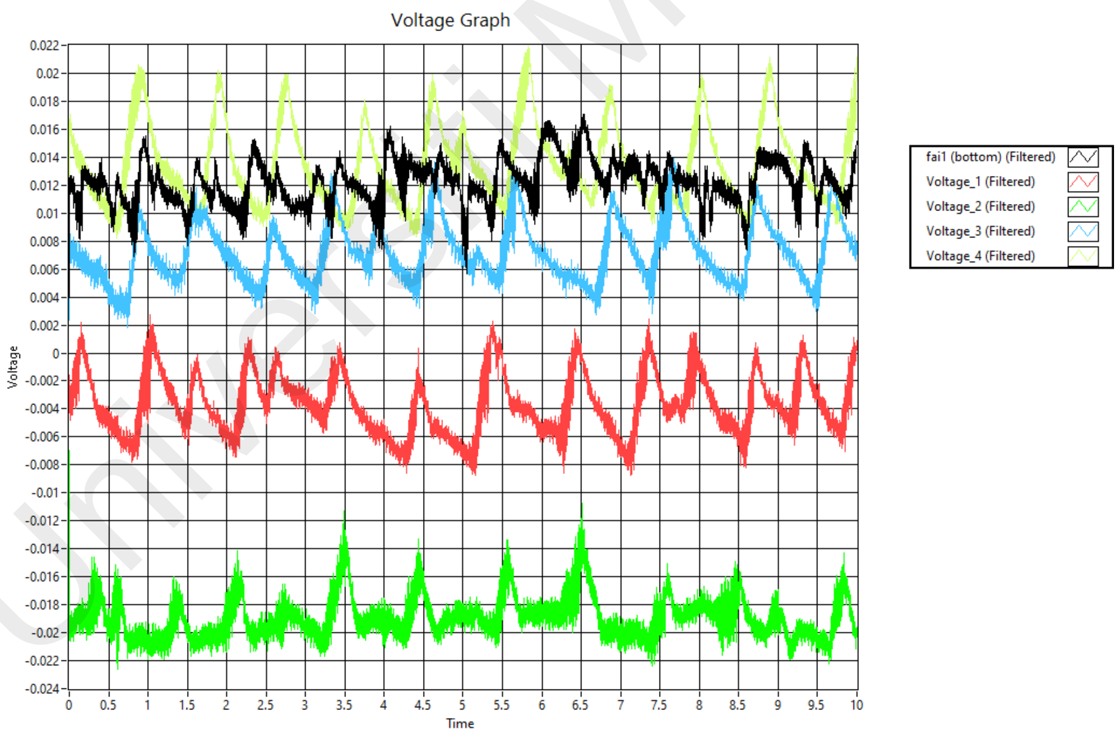

Figure 0.18: Voltage Fluctuation at j_L = 0.227-m/s and j_G = 0.1326-m/s.

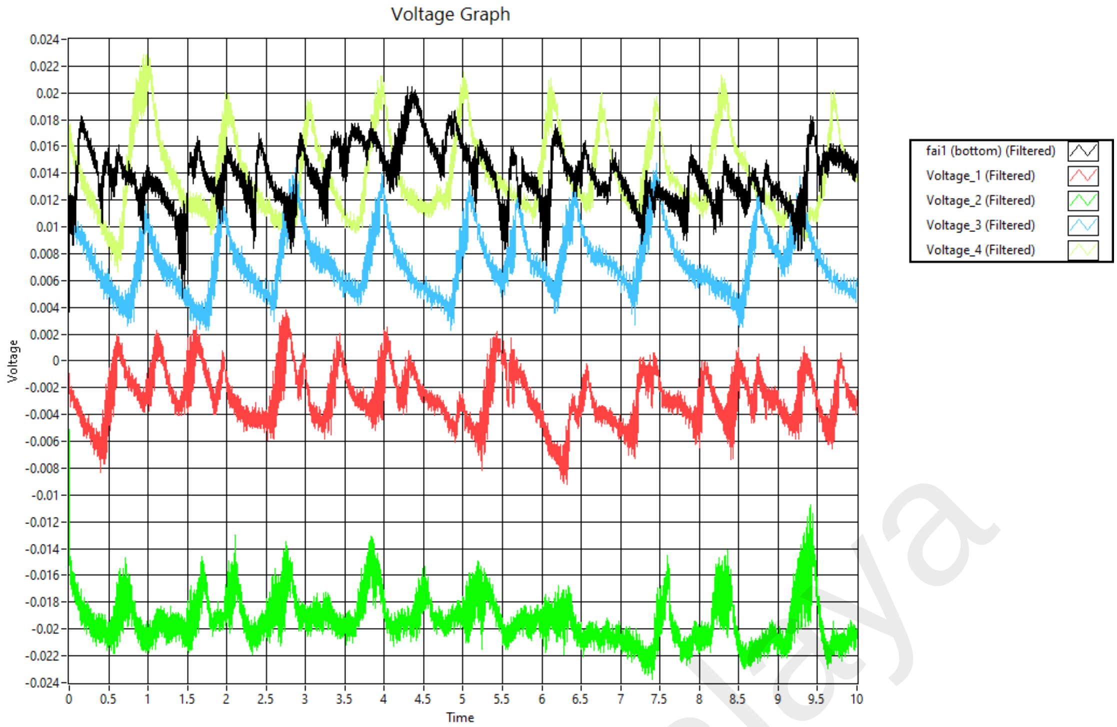

Figure 0.19: Voltage Fluctuation at j_L = 0.227-m/s and j_G = 0.1658-m/s.

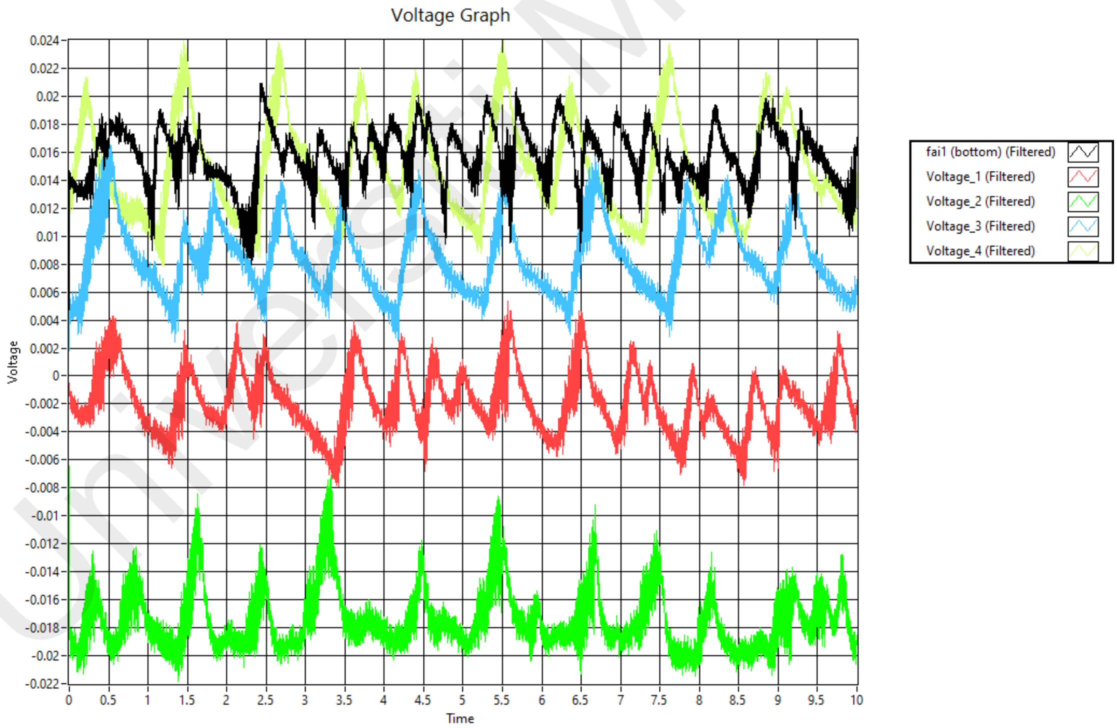

Figure 0.20: Voltage Fluctuation at j_L = 0.227-m/s and j_G = 0.1989-m/s.

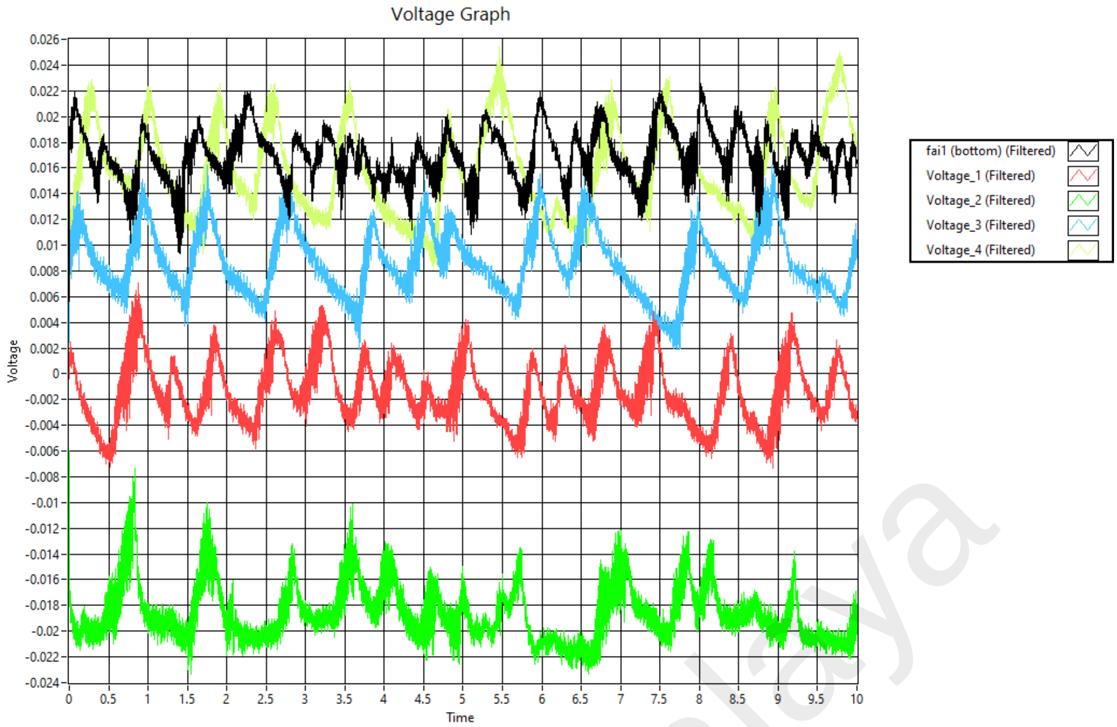

Figure 0.21: Voltage Fluctuation at j_L = 0.227-m/s and j_G = 0.2321-m/s.

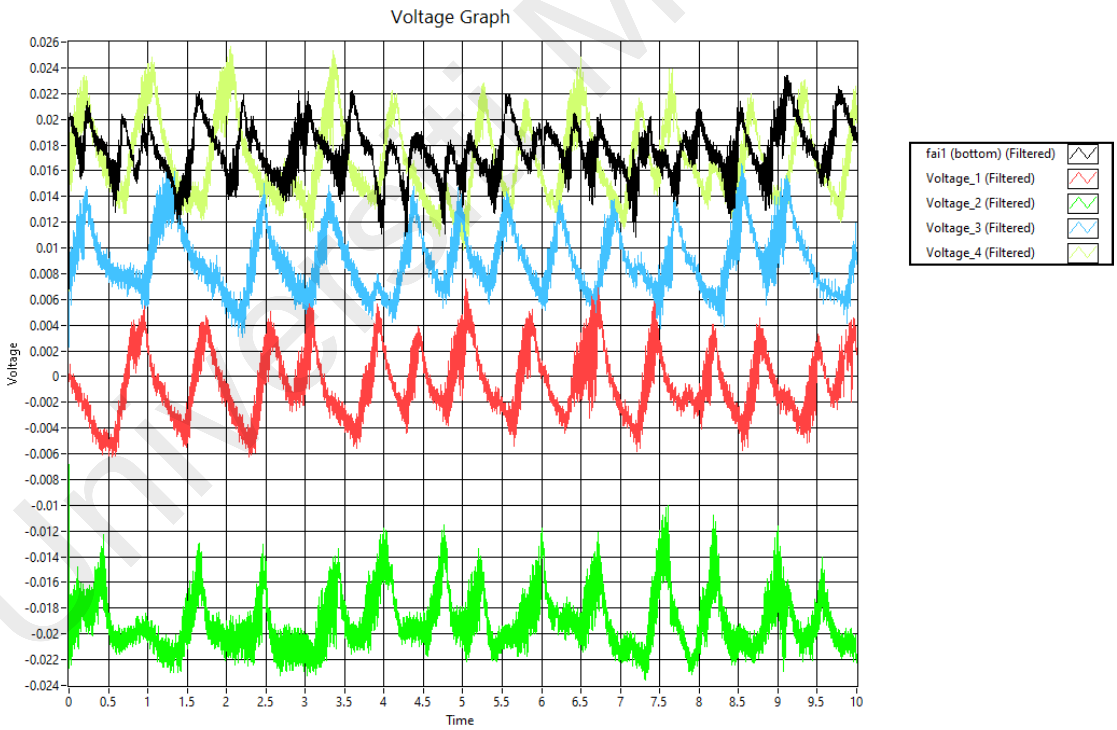

Figure 0.22: Voltage Fluctuation at j_L = 0.227-m/s and j_G = 0.2653-m/s.

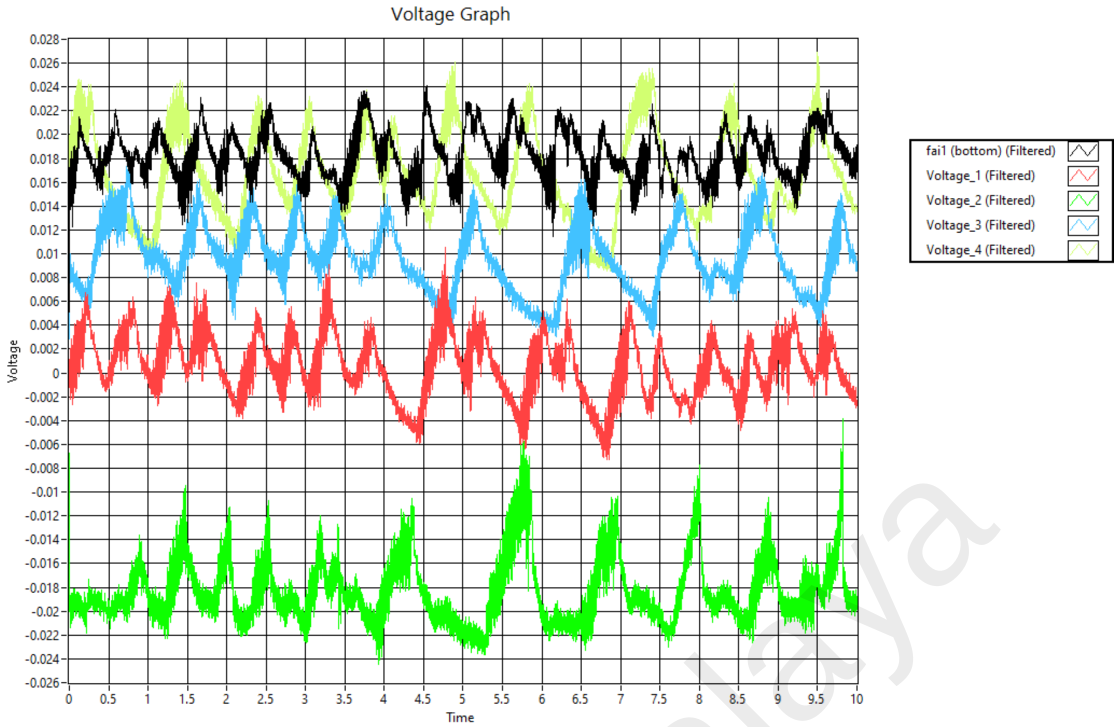

Figure 0.23: Voltage Fluctuation at j_L = 0.227-m/s and j_G = 0.3316-m/s.

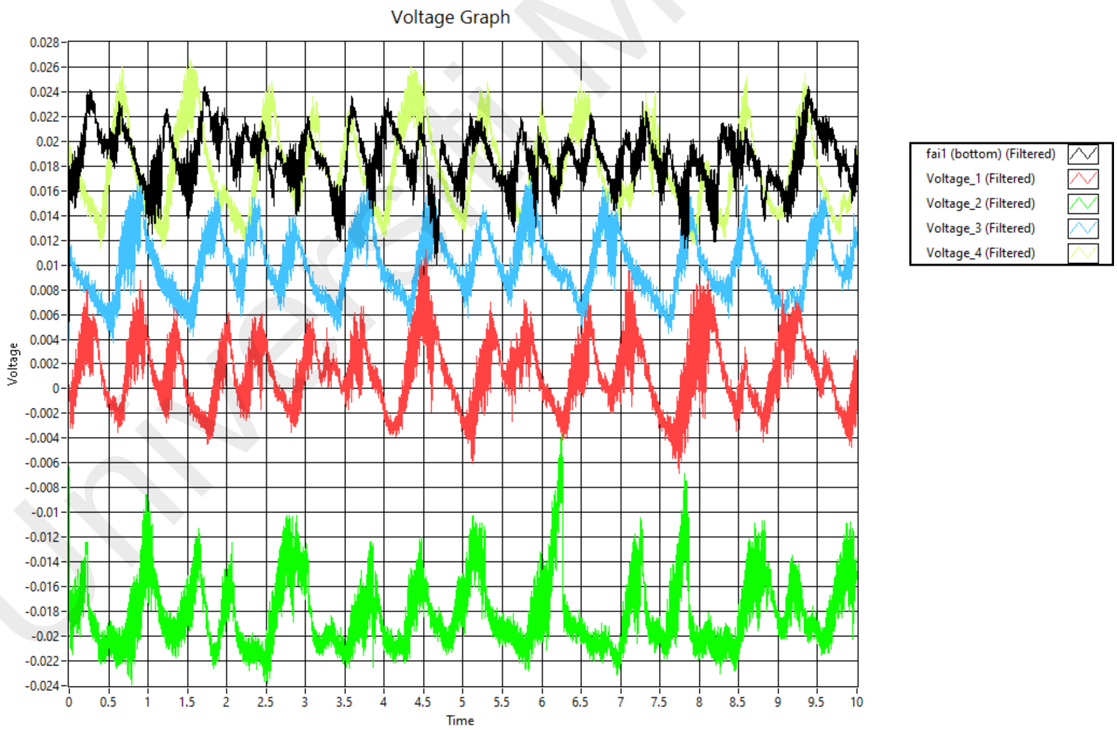

Figure 0.24: Voltage Fluctuation at j_L = 0.227-m/s and j_G = 0.3979-m/s.

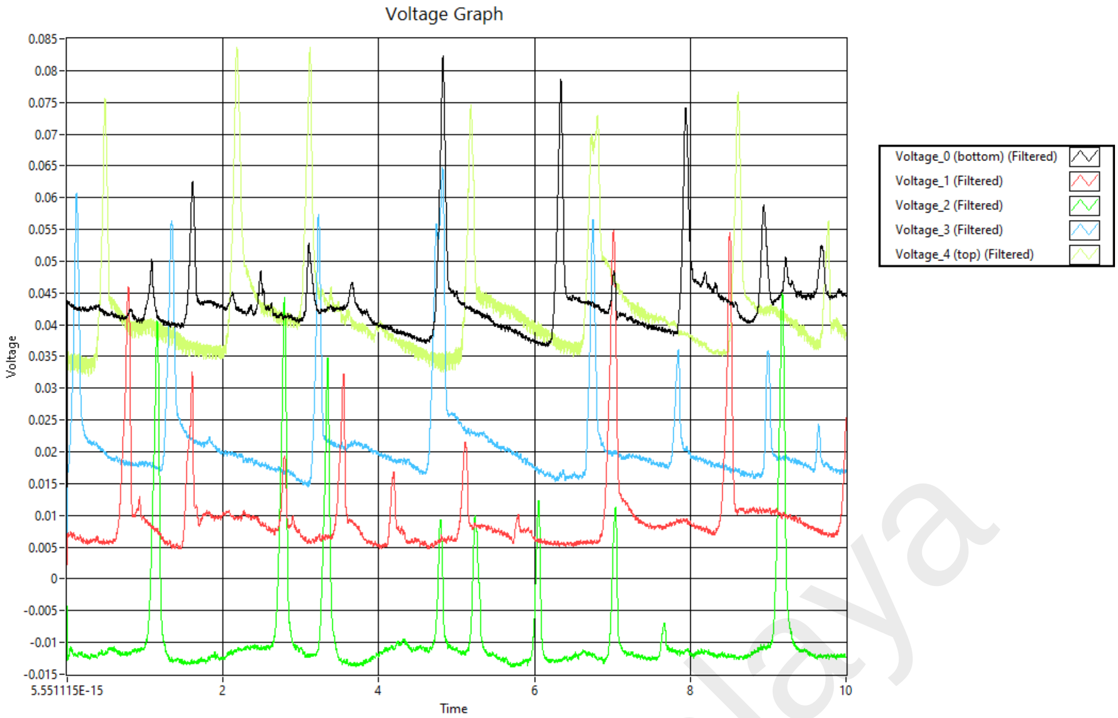

Figure 0.25: Voltage Fluctuation at j_L = 0.397-m/s and j_G = 0.0265-m/s.

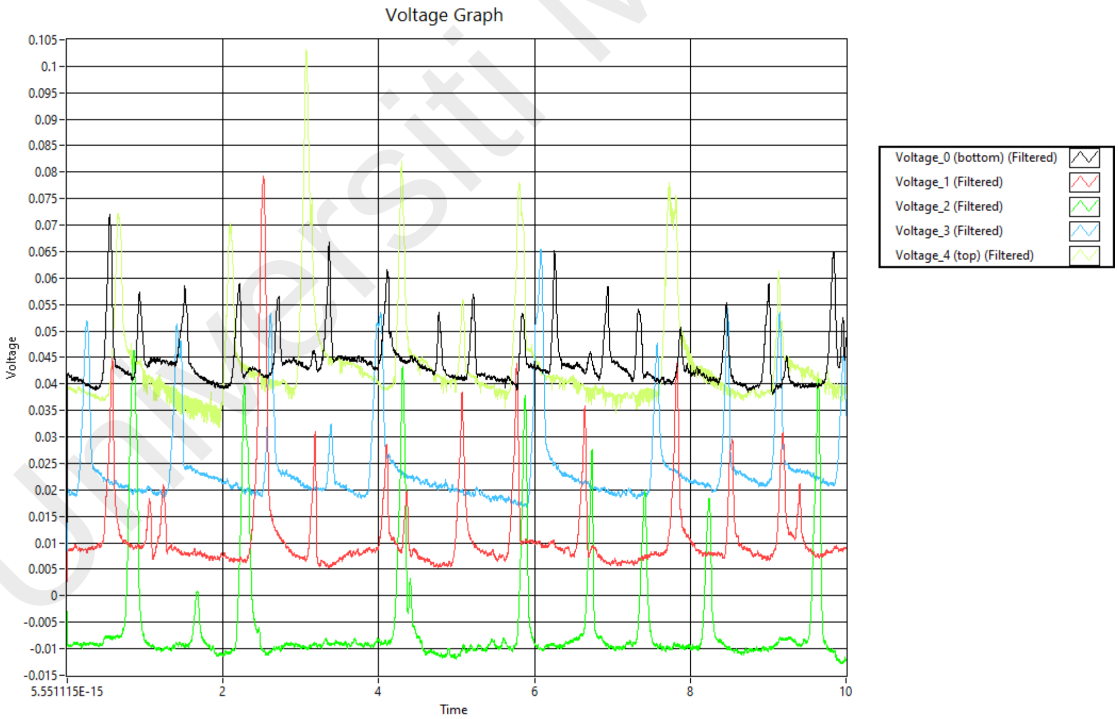

Figure 0.26: Voltage Fluctuation at j_L = 0.397-m/s and j_G = 0.0398-m/s.

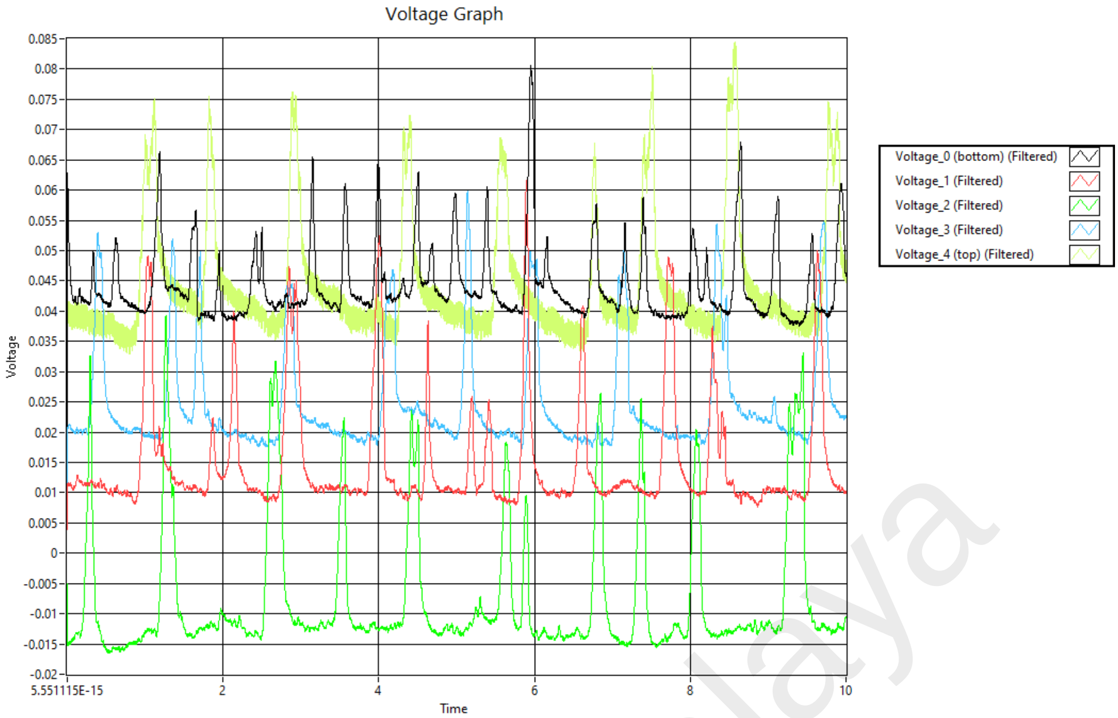

Figure 0.27: Voltage Fluctuation at j_L = 0.397-m/s and j_G = 0.0663-m/s.

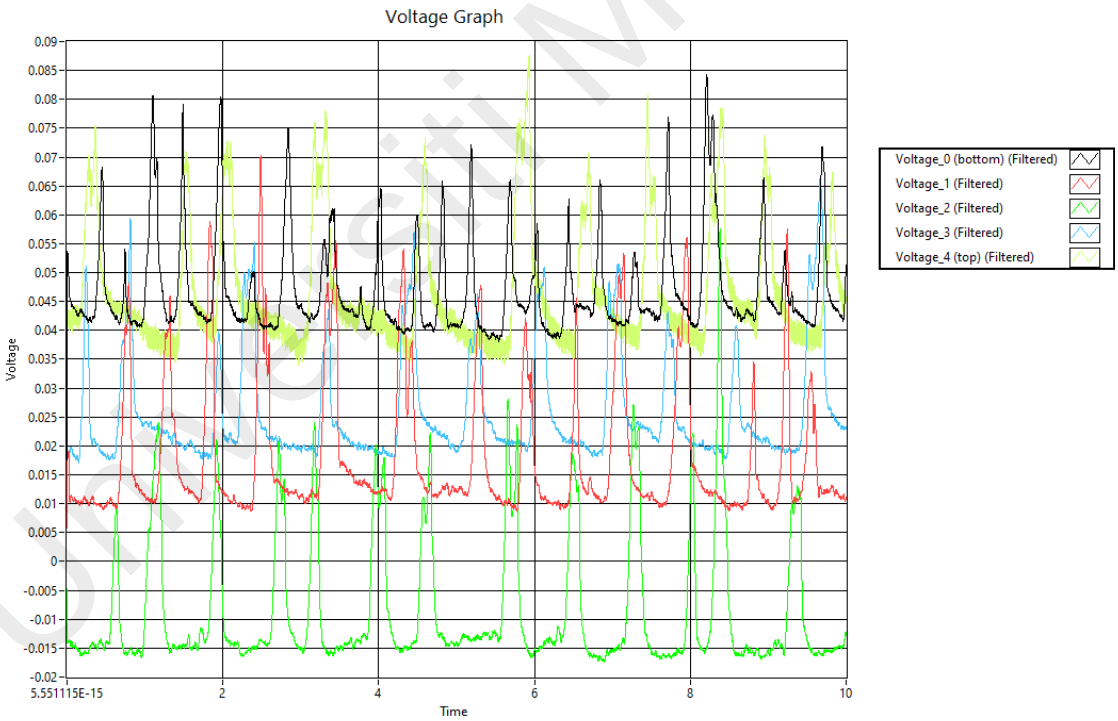

Figure 0. 28: Voltage Fluctuation at j_L = 0.397-m/s and j_G = 0.0995-m/s.

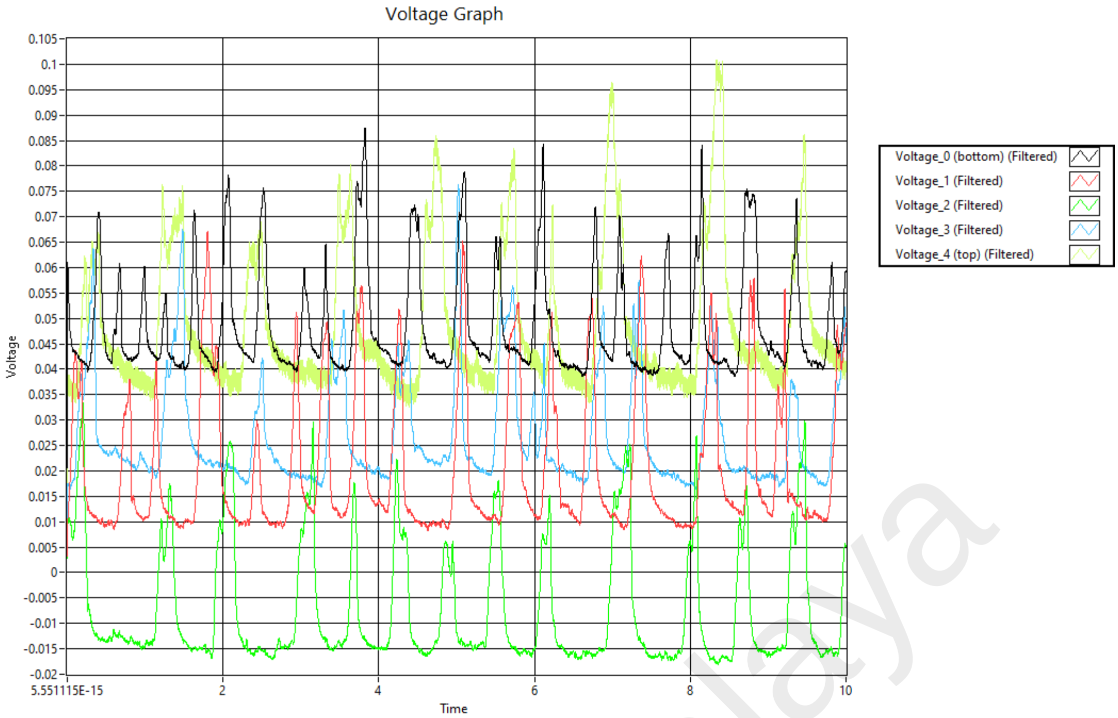

Figure 0.29: Voltage Fluctuation at j_L = 0.397-m/s and j_G = 0.1326-m/s.

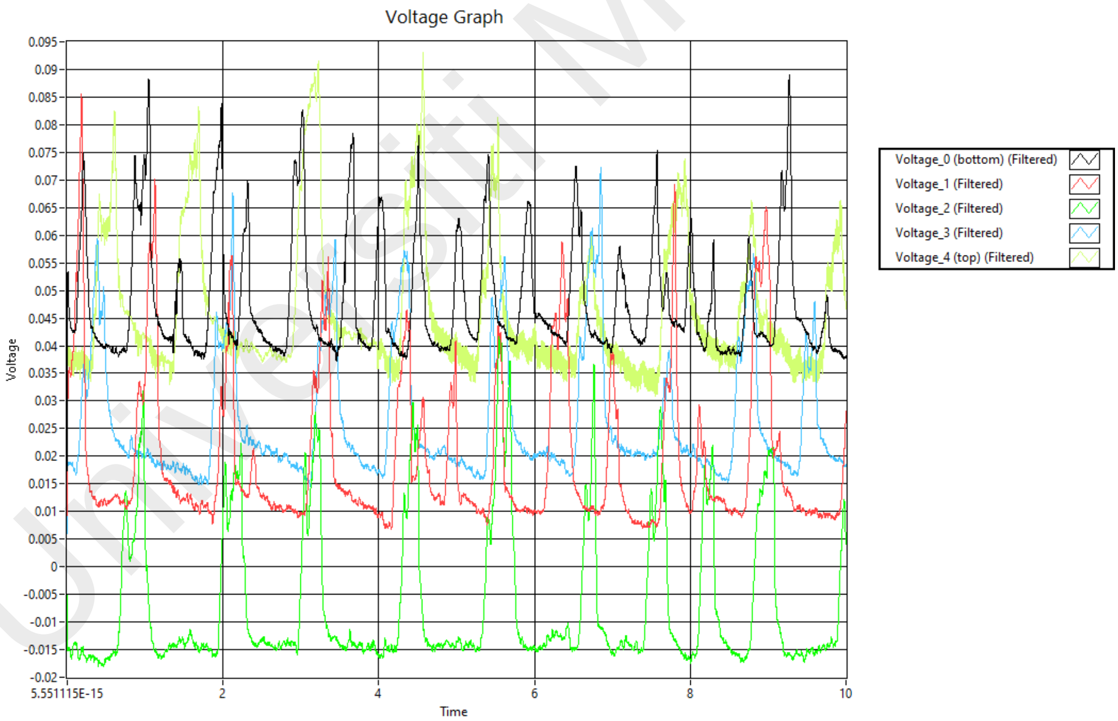

Figure 0. 30: Voltage Fluctuation at j_L = 0.397-m/s and j_G = 0.1658-m/s.

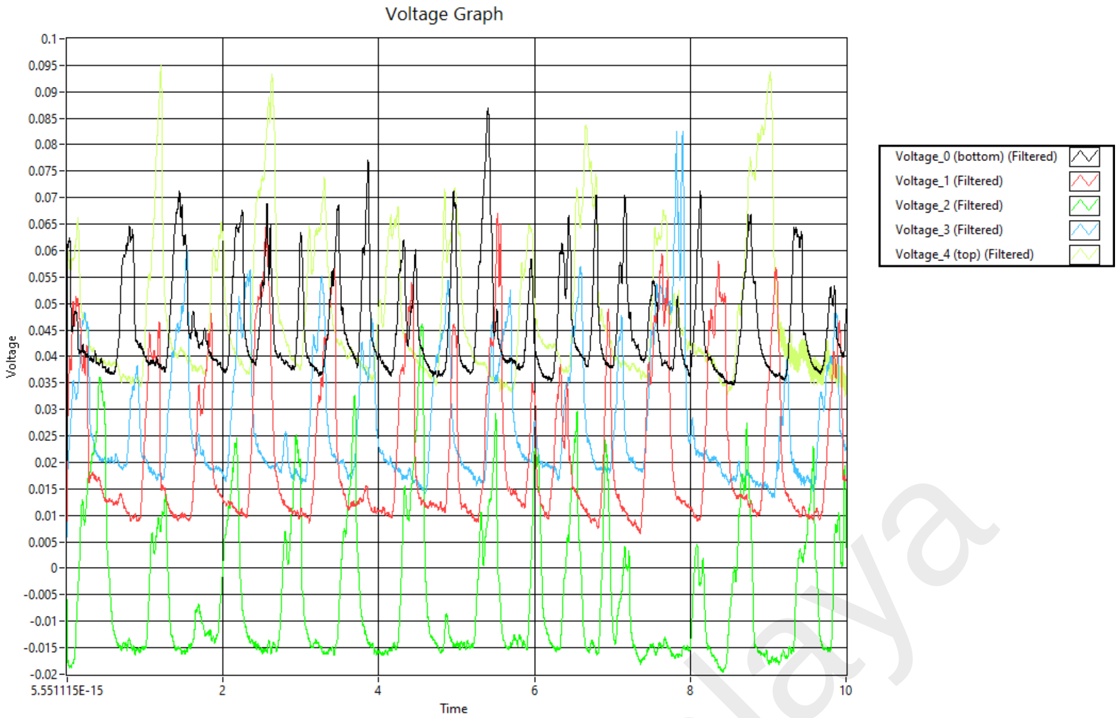

Figure 0.31: Voltage Fluctuation at j_L = 0.397-m/s and j_G = 0.1989-m/s.

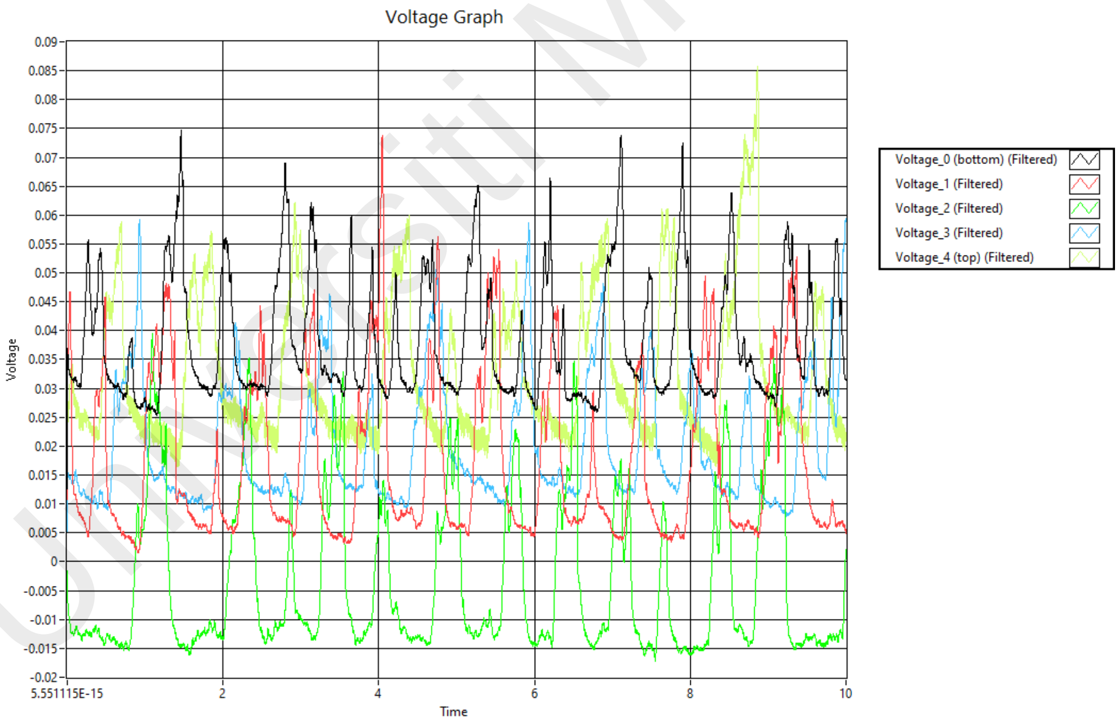

Figure 0.32: Voltage Fluctuation at j_L = 0.397-m/s and j_G = 0.2321-m/s.

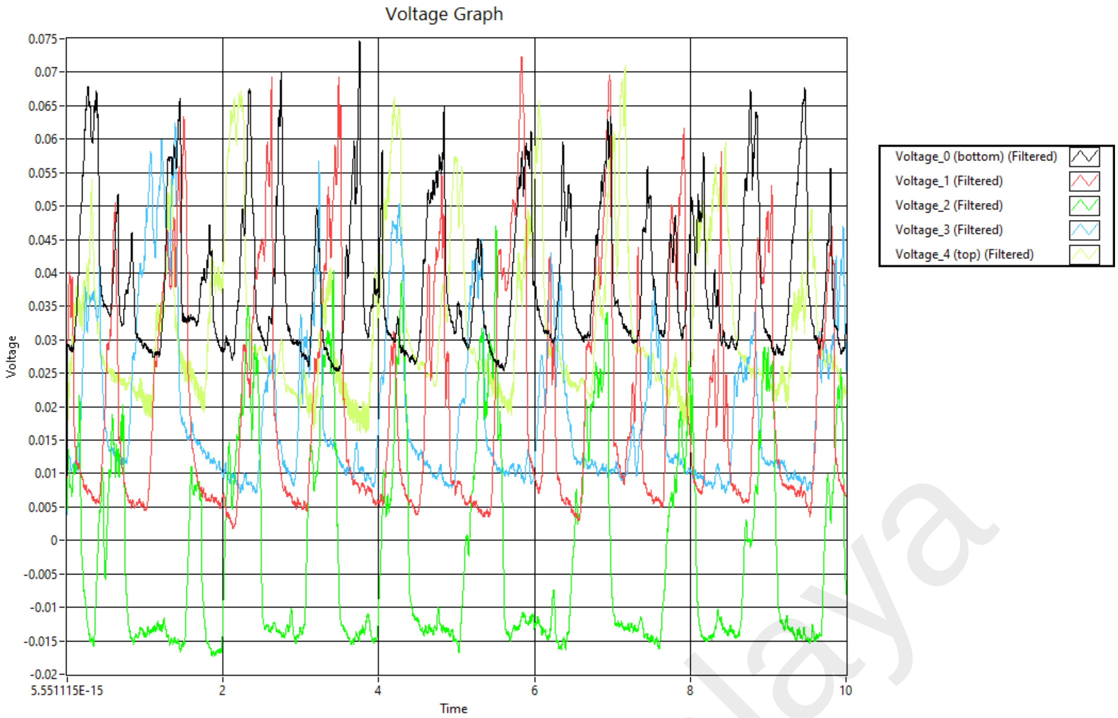

Figure 0.33: Voltage Fluctuation at j_L = 0.397-m/s and j_G = 0.2653-m/s.

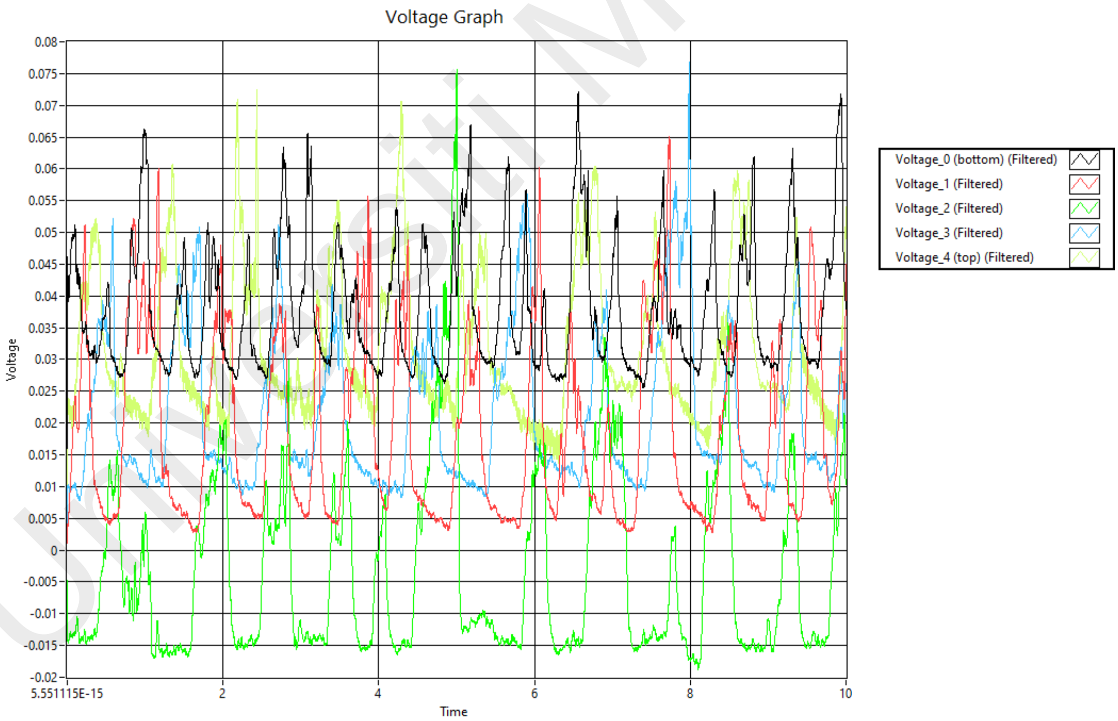

Figure 0.34: Voltage Fluctuation at j_L = 0.397-m/s and j_G = 0.3316-m/s.

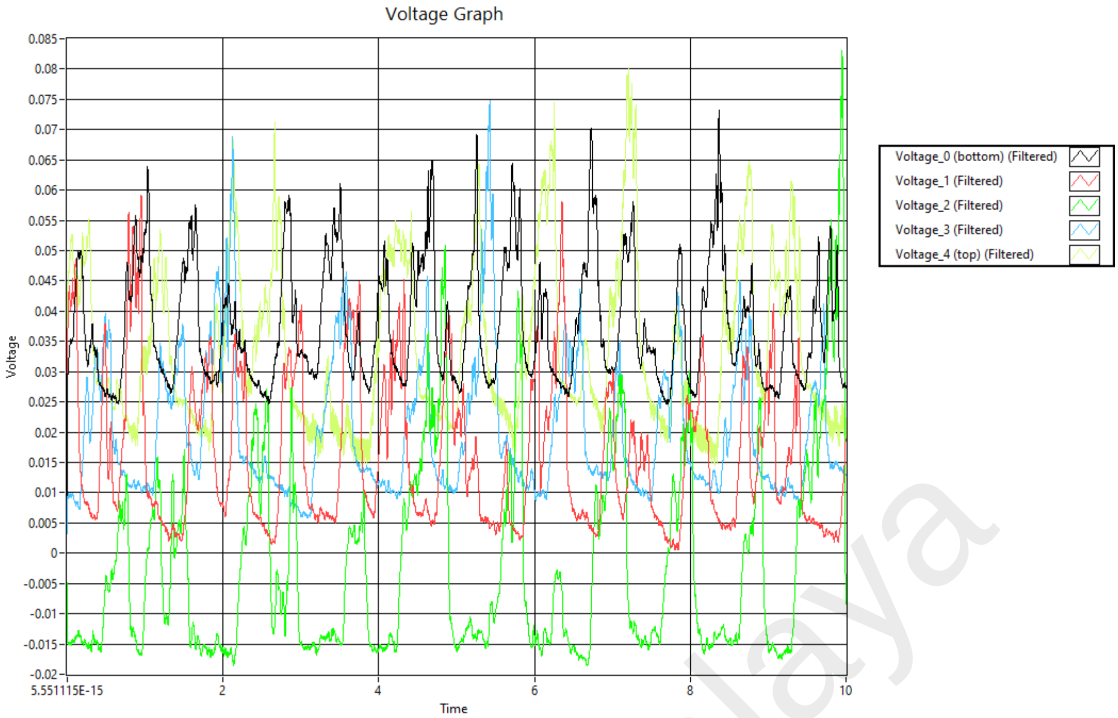

Figure 0.35: Voltage Fluctuation at j_L = 0.397-m/s and j_G = 0.3979-m/s.

REFERENCES

Chang, F., Hu, Z., Li, X., Feng, Z., Ni, S., & Li, H. (2020). Electromagnetic-conductance measurement method for the flow rate and void fraction of gas-liquid two-phase flows. *Measurement: Sensors*, 10–12, 100030. https://doi.org/10.1016/j.measen.2020.100030

Faghri, A., & Zhang, Y. (2010). *Transport phenomena in multiphase systems*. Elsevier Academic Press.

Hampel, U., Barthel, F., Bieberle, A., Bieberle, M., Boden, S., Franz, R., Neumann-Kipping, M., & Tas-Köhler, S. (2020). Tomographic imaging of two-phase flow. *International Journal of Advanced Nuclear Reactor Design and Technology, 2*, 86–92. https://doi.org/10.1016/j.jandt.2020.08.002

Hewitt, G. F., & Roberts, D. (1969). *Studies of two-phase flow patterns by simultaneous x-ray and flast photography.*

Holland, F.A., & Bragg, R. (1995). *Fluid Flow for Chemical Engineers* (pp. 219 – 267). Elsevier.

Hughmark, G. A. (1962). Holdup in gas liquid two-phase flow, *Chem. Eng. Sci.* 20, pp. 1007-1010

Incropera, F. P. (2006). *Fundamentals of Heat and Mass Transfer 6th Edition with IHT/FEHT 3.0 CD with User Guide Set* (6th ed.). Wiley.

Ismail, N. F.F, Relationship Between Induced Vibration and Void Fraction In a Vertical Gas-Liquid Two-Phase Flow, Bachelor of Engineering (Mechanical) Thesis, University of Malaya, 2021.

Luo, Y., & Daley, S. (2007). *Fault Detection, Supervision and Safety of Technical Processes 2006.* Elsevier Science.

Pai, M. G. (2007). Probability density function formalism for multiphase flows. *Retrospective Theses and Dissertations.* 15917.

Sekoguchi, K., & Takeishi, M. (1989). Interfacial structures in upward huge wave flow and annular flow regimes, *Int. J. of Multiphase Flow,* Vol. 15 (3), pp. 295-305.

Slavič, J., Boltezar, M., Mrsnik, M., Cesnik, M., & Javh, J. (2020). *Vibration Fatigue by Spectral Methods: From Structural Dynamics to Fatigue Damage – Theory and Experiments* (1st ed.). Elsevier.

Uesawa, S. I., Kaneko, A., & Abe, Y. (2012). Measurement of void fraction in dispersed bubbly flow containing micro-bubbles with the constant electric current method. *Flow Measurement and Instrumentation, 24, 50–62.* https://doi.org/10.1016/j.flowmeasinst.2012.03.010

Wallis, G., 1969. One-dimensional two-phase flow, McGraw Hill Publication (Text); 1st Edition, 5th Printing edition (August 1979).

Zainon, M. Z., Zubir, M. A., & Ramli, R. (2014). Velocities Effects on the Void Fraction Distribution in a Vertical Gas-Liquid Two-Phase Flow Channel. *Advanced Materials Research,* Vols. 889-890, pp 369-373.

Zubir, M. A., Ramli, R., and Zainon, M. Z. (2019). Determination of Flow Patterns in Vertical Upward Two-Phase Flow Channel via Void Fraction Profile. *Journal of Applied Fluid Mechanics*, 12(2), 474-483.